

1 **Late Paleocene – early Eocene Arctic Ocean Sea Surface Temperatures:**
2 **reassessing biomarker paleothermometry at Lomonosov Ridge**

3

4 Appy Sluijs¹, Joost Frielin¹, Gordon N. Inglis²*, Klaas G.J. Nierop¹, Francien Peterse¹,
5 Francesca Sangiorgi¹ and Stefan Schouten^{1,3}

6

7 ¹Department of Earth Sciences, Faculty of Geosciences, Utrecht University.

8 Princetonlaan 8a, 3584 CB Utrecht, The Netherlands

9 ²Organic Geochemistry Unit, School of Chemistry, School of Earth Sciences,
10 University of Bristol, Bristol, UK

11 ³NIOZ Royal Institute for Sea Research, Department of Microbiology and
12 Biogeochemistry, and Utrecht University, PO Box 59, 1790AB Den Burg, The
13 Netherlands

14

15 * present address: School of Ocean and Earth Science, National Oceanography Centre
16 Southampton, University of Southampton, UK

17

18

19

20 **Abstract**

21 A series of papers shortly following Integrated Ocean Drilling Program Arctic Coring
22 Expedition (ACEX, 2004) on Lomonosov Ridge indicated remarkably high early
23 Eocene sea surface temperatures (SST; ca. 23 to 27 °C) and land air temperatures (ca.
24 17 to 25 °C) based on the distribution of isoprenoid and branched glycerol dialkyl
25 glycerol tetraether (isoGDGT and brGDGT) lipids, respectively. Here, we revisit these
26 results using recent analytical developments – which have led to improved temperature
27 calibrations and the discovery of new temperature-sensitive glycerol monoalkyl
28 glycerol tetraethers (GMGTs) – and currently available proxy constraints.

29 The isoGDGT assemblages support temperature as the dominant variable controlling
30 TEX₈₆ values for most samples. However, contributions of isoGDGTs from land, which
31 we characterize in detail, complicate TEX₈₆ paleothermometry in the late Paleocene
32 and part of the interval between the Paleocene-Eocene Thermal Maximum (PETM; ~56
33 Ma) and Eocene Thermal Maximum 2 (ETM2; ~54 Ma). Background early Eocene
34 SSTs generally exceeded 20 °C, with peak warmth during the PETM (~26 °C) and
35 ETM2 (~27 °C). We find abundant branched GMGTs, likely dominantly marine in
36 origin, and their distribution responds to environmental change. Further modern work
37 is required to test to what extent temperature and other environmental factors determine
38 their distribution.

39 Published Arctic vegetation reconstructions indicate coldest month mean continental
40 air temperatures of 6-13 °C, which reinforces the question if TEX₈₆-derived SSTs in
41 the Paleogene Arctic are skewed towards the summer season. The exact meaning of
42 TEX₈₆ in the Paleogene Arctic thus remains a fundamental issue, and one that limits
43 our assessment of the performance of fully-coupled climate models under greenhouse
44 conditions.

45 **1. Introduction**

46 The Eocene epoch (56 to 34 million years ago; Ma) has long been characterized by
47 warm climates. The earliest signs of a balmy Eocene Arctic region – fossil leaves of
48 numerous plant species – were documented 150 years ago (Heer, 1869). Subsequent
49 findings identified palms, baobab and mangroves, indicating the growth of temperate
50 rainforests and year-round frost-free conditions in the Eocene Arctic region
51 (Schweitzer, 1980; Greenwood and Wing, 1995; Suan et al., 2017; Willard et al., 2019).
52 Fossils of animals, including varanid lizards, tortoises and alligators also indicate warm
53 Arctic climates (Dawson et al., 1976; Estes and Hutchinson, 1980). These earliest
54 findings sparked interest into the climatological mechanisms allowing for such polar
55 warmth about a century ago (Berry, 1922). Ever since, paleobotanists have focused on
56 the Arctic plant fossils and have significantly refined their paleoclimatological
57 interpretation towards estimates of precipitation as well as seasonal and mean annual
58 temperature (e.g. Uhl et al., 2007; Greenwood et al., 2010; Eberle and Greenwood,
59 2012; Suan et al., 2017; Willard et al., 2019).

60 Novel insights in Paleogene Arctic paleoclimate research were made in the years
61 following the Arctic Coring Expedition 302 (ACEX, Integrated Ocean Drilling
62 Program (IODP) 2004, Figure 1). This expedition recovered upper Paleocene and lower
63 Eocene siliciclastic sediments, deposited in a shallow marine environment, in Hole 4A
64 ($87^{\circ} 52.00' \text{N}$; $136^{\circ} 10.64' \text{E}$; 1,288 m water depth), on the Lomonosov Ridge in the
65 central Arctic Ocean (Backman et al., 2006). The succession was deposited at a
66 paleolatitude of $\sim 78^{\circ} \text{N}$, based on a geological reconstruction (Seton et al., 2012)
67 projected using a paleomagnetic reference frame (Torsvik et al., 2012) (see
68 paleolatitude.org, Van Hinsbergen et al., 2015). The sediments are devoid of biogenic
69 calcium carbonate, but rich in immature organic matter, including terrestrial and marine

70 microfossil assemblages and molecular fossils (e.g. Pagani et al., 2006; Sluijs et al.,
71 2006; Stein et al., 2006).

72 As the upper Paleocene and lower Eocene sediments of the ACEX core lack biogenic
73 calcium carbonate and alkenones, SST reconstructions are based on the biomarker-
74 based paleothermometer TEX_{86} . This proxy is based on membrane lipids (isoprenoid
75 glycerol dibiphytanyl glycerol tetraethers; isoGDGTs) of Thaumarchaeota, which adapt
76 the fluidity of their membrane according to the surrounding temperature by increasing
77 the number of cyclopentane rings at higher temperatures (De Rosa et al., 1980; Wuchter
78 et al., 2004; Schouten et al., 2013, and references therein). The proxy was introduced
79 in 2002 by Schouten et al. (2002) and was calibrated to mean annual SST using modern
80 marine surface sediments.

81 Initial papers suggested that Arctic SST increased significantly during two episodes of
82 transient global warming. Maximum values of $\sim 23^\circ\text{C}$ and $\sim 27^\circ\text{C}$ occurred during the
83 Paleocene-Eocene Thermal Maximum (PETM-56 Ma ago, Sluijs et al., 2006) and
84 Eocene Thermal Maximum 2 (ETM2-54 Ma ago, Sluijs et al., 2009), respectively.
85 Lower SSTs, generally exceeding 20°C , characterized the remainder of the early
86 Eocene (Sluijs et al., 2008b). Such temperatures were immediately recognized to be
87 remarkably high and could not be explained using fully-coupled climate model
88 simulations (Sluijs et al., 2006). Even the current-generation of IPCC-class models are
89 unable to match early Eocene Arctic mean annual SSTs, although reconstructions of
90 tropical and mid-latitude SSTs and deep ocean temperatures are consistent with some
91 newer simulations (Frieling et al., 2017; Cramwinckel et al., 2018; Evans et al., 2018;
92 Zhu et al., 2019).

93 Since the publication of the ACEX SST records, constraints on the applicability of the
94 TEX_{86} proxy have tremendously improved (see review by Schouten et al., 2013, and

95 subsequent work by Taylor, 2013 #1645; Elling et al., 2014; Qin et al., 2014; Elling et
96 al., 2015; Kim et al., 2015; Qin et al., 2015; Hurley et al., 2016; Zhang et al., 2016).
97 This work has delivered new constraints on the ecology of Thaumarchaeota, the
98 dominant depth at which they reside in the ocean and from which depth their isoGDGTs
99 are exported towards the sea floor. It also identified potential confounding factors such
100 as variation in dominant isoGDGT export depth (e.g., Taylor et al., 2013; Kim et al.,
101 2015), the input of non-Thaumarchaeotal-derived isoGDGTs (e.g., Weijers et al., 2011;
102 Zhang et al., 2011), growth phase (Elling et al., 2014), and environmental ammonium
103 and oxygen concentrations (Qin et al., 2015; Hurley et al., 2016). Moreover, several
104 indicators to detect such anomalies have been developed. Improvements in the
105 chromatography method used for GDGT analysis now allow for better separation of
106 previously co-eluting compounds leading to enhanced analytical precision and
107 sensitivity (Hopmans et al., 2016). Finally, recent work has described new GDGTs from
108 oceans and sediments, notably branched glycerol monoalkyl glycerol tetraethers
109 (brGMGTs, or ‘H-shaped’ brGDGTs) (e.g., Schouten et al., 2008; Liu et al., 2012),
110 characterized by a covalent carbon-carbon bond that links the two alkyl chains. Their
111 presence and distribution in peats and lake sediments has been linked to land air
112 temperatures (LAT) (e.g., Naafs et al., 2018a; Baxter et al., 2019). However, these
113 compounds have not yet been reported from ancient marine sediments.
114 Considering these developments and the paleoclimatological importance of the ACEX
115 dataset, we re-analyzed the original lipid extracts for the PETM, ETM2 and the interval
116 spanning these events (Sluijs et al., 2006; Sluijs et al., 2009), according to the latest
117 chromatography protocols. We also compile published and generate new GDGT data
118 from modern and Paleogene terrestrial deposits and use these to better assess the

119 potential confounding influence of isoGDGTs from terrestrial sources, which was
120 already recognized as a potential problem in the early work (Sluijs et al., 2006).

121

122 **2. GDGT-based SST indices, calibration and confounding factors**

123 *2.1 TEX₈₆ and its calibration to SST*

124 TEX₈₆ is based on the relative abundance of 4 different GDGTs (Figure 2), following
125 (Schouten et al., 2002):

126
$$TEX_{86} = \frac{([GDGT-2]+[GDGT-3]+[Crenarchaeol\ isomer])}{([GDGT-1]+[GDGT-2]+[GDGT-3]+[Crenarchaeol\ isomer])} \quad \text{Eq. (1)}$$

127 where a higher relative abundance of cyclopentane moieties implies higher SSTs.

128

129 A number of models are used to calibrate TEX₈₆ to SST (Schouten et al., 2002;
130 Schouten et al., 2003; Schouten et al., 2007; Kim et al., 2008; Liu et al., 2009; Kim et
131 al., 2010; Tierney and Tingley, 2014; O'Brien et al., 2017), all based on a modern ocean
132 surface sediment database. The currently available culture and mesocosm experiments
133 and surface sediment data suggest that the relation between SST and TEX₈₆ is close to
134 linear for a large portion of the modern ocean (Kim et al., 2010; Ho et al., 2014; Tierney
135 and Tingley, 2014; O'Brien et al., 2017). In polar regions, the TEX₈₆ response to
136 temperature diminishes (e.g., Kim et al., 2010; Tierney and Tingley, 2014). The
137 response of TEX₈₆ to SST at the high temperature end remains subject of discussion
138 (e.g. Cramwinckel et al., 2018; Hollis et al., 2019). Several authors prefer a linear
139 relation (e.g., Tierney and Tingley, 2014; O'Brien et al., 2017). However, physiological
140 considerations and multiple temperature-dependent GDGT indices might imply a non-
141 linear relation also at the high temperature end, as can be observed at the high end of
142 the modern ocean dataset and beyond the reach of the modern ocean in paleoclimate
143 data (Cramwinckel et al., 2018). At higher temperatures, membrane adaptation may

144 increasingly be established using isoGDGTs not included in the TEX_{86} ratio leading to
145 a diminished TEX_{86} response at very high temperatures (Cramwinckel et al., 2018). A
146 non-linear response has thus been proposed in other calibrations (Liu et al., 2009; Kim
147 et al., 2010). The most recent non-linear calibration, TEX_{86}^H (Kim et al., 2010),
148 represents an exponential relation between SST and TEX_{86} (Hollis et al., 2019).

149 Unfortunately, TEX_{86}^H is mathematically problematic and has systematic residuals in
150 the modern ocean (Tierney and Tingley, 2014).

151 Tierney and Tingley (2014) introduced a spatially-varying Bayesian method to convert
152 TEX_{86} to SST and assumes a linear relationship (BAYSPAR). BAYSPAR extracts
153 TEX_{86} values from the modern core-top dataset that are similar to the measured TEX_{86}
154 value from the geological sample based on a tolerance defined by the user, and
155 subsequently calculates regressions based on these core-top data. The uncertainty in
156 SST reflects spatial differences in the correlation coefficient and intercept and the error
157 variance of the regression model.

158 Currently, it is generally encouraged to present results both using a linear and a non-
159 linear function (Hollis et al., 2019). The assumption of a linear or non-linear relation
160 between SST and TEX_{86} leads to very different SST reconstructions for geological
161 samples yielding TEX_{86} values >0.70 (Kim et al., 2010; Tierney and Tingley, 2014;
162 Frieling et al., 2017; O'Brien et al., 2017; Cramwinckel et al., 2018; Hollis et al., 2019).

163 However, TEX_{86} values of the early Eocene ACEX samples (0.5 – 0.7, Sluijs et al.,
164 2006; Sluijs et al., 2008b; Sluijs et al., 2009) are below this value and well above most
165 values observed in the polar regions (Kim et al., 2010; Tierney and Tingley, 2014;
166 O'Brien et al., 2017), indicating that all calibrations will yield similar absolute SST
167 values.

168

169 *2.2 Caveats and confounding factors*

170 Several confounding factors and caveats have been identified that could potentially bias
171 TEX₈₆ data relative to mean annual SST. These notably relate to additions of isoGDGTs
172 that were not produced in the upper water column by Thaumarchaeota, seasonal biases,
173 and choices that are made in the calibration between SST and TEX₈₆. Below we
174 summarize methods that have been developed to assess if isoGDGT distributions might
175 have been biased by confounding factors.

176

177 *2.2.1 isoGDGTs of terrestrial origin*

178 Previous work (Sluijs et al., 2006; Sluijs et al., 2008b; Sluijs et al., 2009) recognized
179 that high contributions of terrestrially-derived isoGDGTs could compromise the TEX₈₆
180 signal for portions of the upper Paleocene to lower Eocene interval of the ACEX core.
181 This contribution can be tracked using the Branched and Isoprenoid Tetraether (BIT)
182 index, a ratio of mostly soil-derived branched GDGTs (brGDGTs; Figure 2) and
183 Crenarchaeol, which is dominantly marine-derived (Hopmans et al., 2004; Schouten et
184 al., 2013):

$$185 \text{BIT index} = \frac{([brGDGT-Ia] + [brGDGT-IIa] + [brGDGT-IIIa])}{([brGDGT-Ia] + [brGDGT-IIa] + [brGDGT-IIIa] + [Crenarchaeol])} \quad \text{Eq. (2)}$$

186 Most studies define a BIT value (typically 0.3 or 0.4) above which TEX₈₆-derived SST
187 are unreliable (e.g., Weijers et al., 2006). However, the threshold of 0.4 is conservative
188 in some settings and the impact of terrigenous GDGTs on reconstructed SST will
189 depend on the nature and temperature of the source catchment (Inglis et al., 2015). In
190 addition, a cut-off value based on BIT values is difficult given the relatively large
191 differences in BIT between labs, which originate from methodological differences
192 (Schouten et al., 2009). A strong linear relationship between BIT and TEX₈₆ values is
193 often taken as indication of a bias in TEX₈₆ through land-derived isoGDGTs to the

194 marine TEX₈₆ signature (e.g., Douglas et al., 2014). An earlier study used a somewhat
195 subjective threshold of 0.3 for an interval spanning ETM2 in the ACEX core (Sluijs et
196 al., 2009).

197

198 *2.2.2 isoGDGTs of deep water origin*

199 Thaumarchaeota, the source of most isoGDGTs in marine waters (Zeng et al., 2019;
200 Besseling et al., 2020), are ammonium oxidizers (Könneke et al., 2005; Wuchter et al.,
201 2006a), making them independent of light. Although they occur throughout the water
202 column, maximum abundances occur at depths <200 m, generally around NO₂ maxima
203 (e.g., Karner et al., 2001; Pitcher et al., 2011a). In most oceans, sedimentary GDGTs
204 dominantly derive from the upper few hundred meters, based on analyses of suspended
205 particular organic matter and sediment traps (Wuchter et al., 2005; Wuchter et al.,
206 2006b; Yamamoto et al., 2012; Richey and Tierney, 2016). A deeper contribution has
207 also been inferred based on ¹⁴C analysis (Shah et al., 2008), implying possible
208 contributions of isoGDGTs from thermocline. Moreover, contributions of isoGDGTs
209 produced in the deep sea have regionally been identified (e.g., Kim et al., 2015). Taylor
210 et al. (2013) also found that deep dwelling (>1000 meter) archaea might contribute to
211 the sedimentary isoGDGT assemblage. They indicate that such deep contributions can
212 be tracked using the GDGT-2/GDGT-3 ratio; high values of >5 indicate contributions
213 of archaea living deeper in the water column. Given that upper Paleocene and lower
214 Eocene ACEX sediments were deposited in a shallow shelf environment (Sluijs et al.,
215 2008b), a significant contribution of deep ocean archaeal lipids is not expected.

216

217 2.2.3 *isoGDGTs of methanotrophic and methanogenic archaea*

218 Contributions of isoGDGTs to the sedimentary pool might also derive from anaerobic
219 methanotrophs and/or methanogens. Several indices have been developed to track such
220 contributions, both based on relatively high contributions of particular isoGDGTs of
221 these groups of archaea. The Methane Index (MI) was developed to detect the relative
222 contribution of anaerobic methanotrophic Euryarchaeota assumed to be represented by
223 GDGT-0 but also GDGT-1, 2 and 3 (Zhang et al., 2011) and is therefore defined as

224
$$MI = \frac{[GDGT-1]+[GDGT-2]+[GDGT-3]}{([GDGT-1]+[GDGT-2]+[GDGT-3]+[Crenarchaeol]+[Crenarchaeol\ isomer])} \quad \text{Eq. (3)}$$

225 MI values greater than 0.5 indicate significant contribution of anaerobic
226 methanotrophy. Such values may yield unreliable TEX₈₆ values. Another tracer for
227 contributions of anaerobic methanotrophic archaea is the analogous GDGT-
228 2/Crenarchaeol ratio (Weijers et al., 2011).

229 Methanogenic archaea can synthesize GDGT-0, as well as smaller quantities of GDGT-
230 1, GDGT-2 and GDGT-3. The ratio GDGT-0/Crenarchaeol is indicative of
231 contributions of methanogenic archaea to the isoGDGT pool (Blaga et al., 2009) where
232 values > 2 indicate substantial contribution of methanogenic archaea. Up to now, high
233 index values have often been observed near methane seeps or anoxic basins (e.g.,
234 Jaeschke et al., 2012) but rarely in open marine waters in the modern and paleodomains
235 (Inglis et al., 2015; Zhang et al., 2016). Given the reducing conditions in the sediment
236 and water column at the study site across the late Paleocene and early Eocene (Sluijs et
237 al., 2006; Stein et al., 2006; Sluijs et al., 2008b; März et al., 2010), an influence of
238 methane cycling might be expected.

239

240 2.2.4 *iso*GDGTs of the ‘Red Sea Type’

241 Sedimentary *iso*GDGT distributions from the Red Sea are anomalous to other marine
242 settings and are characterised by the low abundance of GDGT-0 and the high abundance
243 of the Crenarchaeol isomer. Presumably, this is due to an endemic Thaumarchaeotal
244 assemblage. The Red Sea *iso*GDGT distribution yields a different relationship between
245 SST and TEX₈₆ (Trommer et al., 2009; Kim et al., 2015). Inglis et al. (2015) attempted
246 to quantify a ‘Red Sea-type’ GDGT distribution in geological samples using the
247 following index:

248
$$\%GDGTrs = \frac{[Crenarchaeol\ isomer]}{([GDGT-0] + [Crenarchaeol\ isomer])} \times 100 \quad \text{Eq. (4)}$$

249 However, as noted by Inglis et al. (2015) this ratio is also strongly SST-dependent such
250 that the Red Sea type GDGT assemblage cannot be discerned from GDGT distributions
251 that occur at high temperatures in normal open marine settings.

252

253 2.2.5 *Seasonal bias*

254 TEX₈₆ is calibrated to mean annual SST. However, particularly in mid and high latitude
255 areas where production and export production is highly seasonal, the sedimentary
256 GDGT distribution might not represent annual mean conditions (Wuchter et al., 2006b;
257 Pitcher et al., 2011b; Mollenhauer et al., 2015; Richey and Tierney, 2016; Park et al.,
258 2019). This issue should partly be reflected in the calibration uncertainty of the modern
259 ocean database (several °C, depending on the calibration and method; see section 2.7).
260 Sluijs et al. (2006; 2008b; 2009) originally argued that the TEX₈₆ results from the
261 ACEX core could be biased towards summer temperature because the export of organic
262 matter from the surface ocean towards the sediment likely peaked during the season of
263 highest production, i.e., the summer. However, we also note that the TEX₈₆-temperature
264 relationship is not improved when using seasonal mean ocean temperatures (Kim et al.,

265 2010; Tierney and Tingley, 2014) and modern observations indicate homogenization
266 of the seasonal cycle at depth (Wuchter et al., 2006b; Yamamoto et al., 2012; Richey
267 and Tierney, 2016), implying that seasonality has relatively limited effect on modern
268 sedimentary TEX_{86} values.

269

270 *2.2.6 Additional isoGDGT-based temperature indicators*

271 The underlying mechanism of TEX_{86} is that isoGDGTs produced at higher SSTs
272 contain more rings than those produced at low SSTs. Although the combination of
273 compounds included in TEX_{86} seems to yield the strongest relation with temperature in
274 the modern ocean (Kim et al., 2010), it implies that isoGDGT ratios other than TEX_{86}
275 also provide insights into SST. One alternative temperature sensitive isoGDGT index
276 is the Ring Index (RI), which represents the weighed number of cyclopentane rings of
277 isoGDGTs 0-3, Crenarchaeol and the Crenarchaeol isomer (Zhang et al., 2016), defined
278 as:

$$279 RI = 0x[\%GDGT - 0] + 1x[\%GDGT - 1] + 2x[\%GDGT - 2] + 3x[\%GDGT - 3] + \\ 280 4x[\%Crenarchaeol + \%Crenarchaeol isomer] \quad \text{Eq. (5)}$$

281 Note that the abundance of GDGT-0 is important for determining the percentage of the
282 other GDGTs of the total isoGDGT pool.

283 The close relation between TEX_{86} and RI can also be used to detect aberrant
284 distributions, including those produced by methanogenic, methanotrophic and
285 terrestrial sources, as these sources typically contribute disproportionate amounts of
286 specific lipids. A RI_{TEX} , calculated from TEX using the polynomial fit of Zhang et al.
287 (2016), is subtracted from the RI to arrive at the ΔRI . Cut-off values for sample
288 deviation from the modern ocean calibration dataset are defined as 95% confidence
289 limits of the RI- TEX relation, or above $|0.3| \Delta\text{RI}$ units.

290 2.3 *H*-shaped branched GDGTs; brGMGTs

291 BrGMGTs (Figure 2) were first identified by Liu et al. (2012) in marine sediments, who
292 identified a single acyclic tetramethylated brGMGT (*m/z* 1020). This compound was
293 later detected within the marine water column and appeared to be abundant within the
294 oxygen minimum zone (Xie et al., 2014). Naafs et al. (2018a) identified a larger suite
295 of brGMGTs (including *m/z* 1048 and 1034), in a quasi-global compilation of modern
296 peat samples. They argued that these compounds were preferentially produced at depth,
297 within the anoxic catotelm. Analogous to the continental paleothermometer based on
298 bacterial brGDGTs produced in surface soils, termed MBT'_{5me} (Weijers et al., 2007b;
299 De Jonge et al., 2014), they showed that the degree of methylation of brGMGTs in peats
300 relates to mean annual air temperature. They calculated the degree of methylation of
301 brGDGTs without cyclopentane moieties, designed for comparison to the methylation
302 of brGMGTs, defined by H-MBT_{acyclic}:

303

304
$$MBT_{acyclic} = \frac{brGDGT-Ia}{(brGDGT-Ia + brGDGT-IIa + GDGT-IIa' + brGDGT-IIIa + brGDGT-IIIa')} \text{ Eq. (6)}$$

305

306
$$H - MBT_{acyclic} = \frac{brGMGT-H1020}{(brGMGT-H1020 + brGMGT-H1034 + brGMGT-1048)} \text{ Eq. (7)}$$

307

308 Based on the strong relation between MBT_{acyclic} and H-MBT_{acyclic} in their peat samples,
309 Naafs et al. (2018a) suggested that the brGMGTs have the same origin as the brGDGTs,
310 presumably Acidobacteria (Sinninghe Damsté et al., 2011; Sinninghe Damsté et al.,
311 2018a). In addition, they showed that the abundance of brGMGTs (relative to the total
312 amount of brGMGTs and brGDGTs) positively correlates with mean annual air
313 temperature, suggesting that the covalent bond in the brGMGTs is used to maintain
314 membrane stability at higher temperature (Naafs et al., 2018a).

315 Baxter et al. (2019) identified a total of seven different brGMGTs from a suite of
316 African lake sediments (Figure 2), and found their relative distribution to correlate to
317 mean annual air temperature. Accordingly, they proposed a proxy for mean annual air
318 temperature termed brGMGT-I (see Figure 2 for the molecular structures referred to
319 here):

320
$$brGMGT - I = \frac{[H1020c] + [H1034a] + [H1034c]}{[H1020b] + [H1020c] + [H1034a] + [H1034c] + [H1048]} \quad \text{Eq. (8)}$$

321

322 **3. Material and Methods**

323 We used the polar fractions previously analyzed by Sluijs et al. (2006; 2009) from the
324 PETM through ETM2 interval at IODP Expedition 302 Hole 4A. These fractions
325 originate from a total lipid extract produced using a Dionex Accelerated Solvent
326 Extractor and fraction separations by Al_2O_3 column chromatography using
327 hexane:dichloromethane (DCM) (9:1, *v/v*) and DCM:methanol (1:1, *v/v*) to yield the
328 apolar and polar fractions, respectively. Polar fractions were re-dissolved in
329 hexane:isopropanol (99:1, *v/v*) and passed through a 0.45- μm polytetrafluoroethylene
330 filter. This fraction was then analyzed by high-performance liquid chromatography
331 (HPLC) and atmospheric pressure chemical ionization–mass spectrometry using an
332 Agilent 1260 Infinity series HPLC system coupled to an Agilent 6130 single-
333 quadrupole mass spectrometer at Utrecht University following Hopmans et al. (2016)
334 to measure the abundance of GDGTs. Based on long-term observation of the in-house
335 standard, the analytical precision for TEX_{86} calculates to ± 0.3 °C in the SST domain.
336 To gain further insights into the potential impact of terrestrial isoGDGT input on TEX_{86}
337 values, we compiled isoGDGT and brGDGTs distributions from modern peats ($n = 473$,
338 Naafs et al., 2017) and early Paleogene lignites ($n = 58$, Naafs et al., 2018b). Note, the
339 fractional abundance of Crenarchaeol isomer was not reported in the early Paleogene

340 dataset of Naafs et al. (2018b). We therefore revisited the original chromatograms from
341 Naafs et al. (2018b) and integrated the crenarchaeol isomer (m/z 1292).

342

343 **4. Results**

344 The new GDGT distributions (Supplementary Table) are consistent with the TEX₈₆ and
345 BIT index data generated over a decade ago using the older analytical HPLC setup
346 (Hopmans et al., 2000; Hopmans et al., 2016) (Figure 3). TEX₈₆ exhibits some scatter
347 but the slope of the regression is 0.98 for the entire dataset, which is indistinguishable
348 from the 1:1 line. The scatter is minor compared to the uncertainties inherent to
349 calibrations that transfer these values to SST. Less scatter is apparent in the BIT record
350 but the original BIT index values were slightly higher than recorded here (~0.5),
351 indicated by a shallower slope of the regression (0.92). This result is consistent with
352 previous analyses with the new analytical setup (Hopmans et al., 2016). This does not
353 impact previous qualitative interpretations of this record (Sluijs et al., 2006; Sluijs et
354 al., 2008b; Sluijs et al., 2009). In the discussion section, we assess indicators of
355 potential confounding factors (section 2.2), including the influx of terrestrially-derived
356 isoGDGTs to the sediments (Figures 4, 5 and S1) and several indices related to methane
357 and depth of production (Figures 6).

358 Although we did not detect significant amounts of isoprenoid GMGTs, high
359 abundances of various brGMGTs are present in the ACEX samples, in total between 10
360 and 45% of the total brGDGT assemblage (Figure 7). We consistently identify at least
361 five brGMGTs across the three different mass-to-charge ratios (m/z 1020, 1034 and
362 1048). Based on their (relative) retention times and overall distribution we were able to
363 apply the nomenclature of Baxter et al. (2019) to five of these and assign individual
364 peaks to previously identified compounds (Figure S2). The abundance of brGMGTs

365 relative to brGDGTs increase during the PETM. The proposed temperature indicators
366 based on brGMGTs show mixed results, with some showing a clear response to the
367 PETM (Figure 7e) while others do not (Figure 7d).

368

369 **5. Discussion**

370 *5.1 IsoGDGT provenance*

371 *5.1.1 Contributions of soil-derived isoGDGTs*

372 As noted by Sluijs et al. (2006), late Paleocene samples yield anomalously high
373 abundances of GDGT-3, likely derived from a terrestrial source. We therefore consider
374 the late Paleocene temperature estimates unreliable. To assess the temperature change
375 during the PETM, Sluijs et al. (2006) developed a TEX_{86} calibration without this
376 moiety, termed TEX'_{86} . However, TEX'_{86} has not been widely used outside the
377 Paleogene Arctic because the anomalous abundances of GDGT-3 have not been
378 recorded elsewhere. High contributions of GDGT-3 from terrestrial input would also
379 be associated with an increase in the abundance of other isoGDGTs. Indeed, recent
380 TEX_{86} -based global SST compilations and comparison to climate simulations for the
381 PETM excluded the Paleocene ACEX data because the TEX_{86}' calibration complicates
382 the comparison to other regions where it has not been applied (Frieling et al., 2017;
383 Hollis et al., 2019).

384 Input of soil organic matter is consistent with Willard et al. (2019) who established that
385 the brGDGT assemblage is dominantly soil-derived as opposed to being produced in
386 the coastal marine environment. This observation is based upon the weighted average
387 number of rings in the tetramethylated brGDGTs ($\#\text{rings}_{\text{tetra}}$) which generally does not
388 exceed 0.4 to 0.7 in the global soil calibration dataset (Sinninghe Damsté, 2016). In the
389 ACEX record, $\#\text{rings}_{\text{tetra}}$ is < 0.21 (Willard et al., 2019), consistent with a dominant soil

390 source. This indicates that 1) brGDGT abundances, 2) brGDGT distributions and 3) the
391 BIT index are reliable indicators of the relative supply of terrestrially-derived
392 isoGDGTs into the marine basin. The Paleocene section of the dataset also stands out
393 regarding its relation between BIT index and TEX₈₆ (Figure 4), which confirms its
394 anomalous nature.

395 During the PETM, TEX₈₆ values are higher (due to warming) and BIT values lower.
396 This was attributed to sea level rise during the hyperthermals resulting in a more distal
397 position relative to the terrestrial GDGT source (Sluijs et al., 2006; Sluijs et al., 2008a).
398 The interval between 371.0 and 369.0 mcd (i.e. above the PETM and below ETM2)
399 stands out. This interval was previously recognized by Sluijs et al. (2009) to reflect an
400 open marine environment, with a dominance of marine palynomorphs and algal
401 biomarkers. They also found that high BIT values correspond to low TEX₈₆ values
402 within that interval and therefore implemented a subjective threshold value of 0.3,
403 above which TEX₈₆-derived SSTs were considered unreliable. Although the relation
404 between BIT and TEX₈₆ exhibits considerable much scatter, the new analyses supports
405 the notion that higher influx of terrestrial isoGDGTs lowers TEX₈₆ values. The linear
406 regression (Figure 4; excluding the one outlier with high TEX₈₆ and BIT values in the
407 top right of the plot because it has highly anomalous distributions ($\Delta RI = 0.61$)), yields
408 an R^2 of 0.26 so explains a portion of the variation (Figure 4). The nature of this
409 influence is determined by the relative abundance of terrestrial isoGDGTs and their
410 TEX₈₆ value. The TEX₈₆ value at the terrestrial endmember of BIT = 1, assuming
411 various types of regressions, centers around 0.5. The remainder of the data does not
412 show a clear relation between BIT and TEX₈₆ although some of the lowest TEX₈₆
413 values correspond to high BIT values, suggesting that the terrestrial endmember

414 contributed isoGDGT assemblages with relatively low TEX₈₆ values in other intervals
415 as well.

416 The relatively low degree of cyclization in the early Eocene contrasts starkly with high
417 degree of cyclisation during the late Paleocene (Figure 6). This implies that the
418 distribution of terrestrial isoGDGTs varies strongly between the latest Paleocene and
419 early Eocene within our studied section.

420 The impact of soil-derived isoGDGTs also emerges from the Ring Index approach of
421 Zhang et al. (2016, see section 2.6 and Figure 6). The difference between the Ring Index
422 and TEX₈₆ at the onset of the PETM is mainly controlled by Crenarchaeol, which is
423 comparatively low in abundance in the Paleocene but highly abundant in the PETM.
424 This increase is likely associated with sea level rise during the PETM because
425 Crenarchaeol is predominantly produced in the marine realm. It is also consistent with
426 a drop in BIT index values and the relative abundance of terrestrial palynomorphs
427 (Sluijs et al., 2008a). The approach of Zhang et al. (2016) also confirms that many
428 isoGDGT distributions exhibit an anomalous relation between TEX₈₆ and the Ring
429 Index relative to the modern core top dataset, with Δ RI values >0.3 (Figure 6).
430 Importantly, all samples with Δ RI values >0.3 have BIT values above 0.35, indicating
431 that contributions of soil-derived iso-GDGTs dominate non-temperature effects in the
432 distributions. We therefore discard TEX₈₆-derived SSTs for samples with BIT values
433 >0.35 .

434 We also develop a crude model to further constrain the potential contribution of
435 terrestrially-derived isoGDGTs. First, we determine the abundance of isoGDGTs
436 relative to brGDGTs in modern peat samples (Naafs et al., 2017) and early Paleogene
437 lignites (fossil peat) (Naafs et al., 2018b, the isoGDGT data are published here).
438 Although there is no reason to assume that peat was a major component of the

439 hinterland (Willard et al., 2019) , the aforementioned datasets can provide an estimate
440 of the potential contribution from terrestrial isoGDGTs to our study site. The raw signal
441 intensity of brGDGTs in the ACEX samples are used to estimate the potential
442 contribution of terrestrially-derived isoGDGTs to the samples. To this end, we use the
443 fractional abundance of the various isoGDGTs in the modern peat and Paleogene lignite
444 datasets (Figure 5). Then, we estimate the abundance of these terrestrially-derived
445 isoGDGTs in our ACEX samples by scaling this fraction to the measured abundances
446 of brGDGTs and isoGDGTs in our ACEX samples, following

447 *Terrestrial fraction of isoGDGT x =*

448
$$\left(\text{Fraction of isoGDGT}_x \text{ in terrestrial test dataset} * \frac{\text{sum(brGDGTs)}}{\text{abundance of isoGDGT } x} \right) \text{ Eq. (9)}$$

449 where x represents the specific analyzed GDGT (see Supplementary Data File for an
450 example of these calculations).

451 This leads to estimates of the potential relative contributions of the individual
452 isoGDGTs derived from land in the ACEX samples based on the entire modern peat
453 dataset (Naafs et al., 2017), modern peats from regions with MAT exceeding 15°C
454 (Naafs et al., 2017) and Paleogene lignites (Naafs et al., 2018b, this paper, Figures 5
455 and S1). This approach implies that Crenarchaeol and the Crenarchaeol-isomer are
456 almost exclusively from the marine realm. However, GDGT-1, GDGT-2 and GDGT-3
457 in our study site may be derived from the terrestrial realm (Figure 5), especially in
458 specific stratigraphic intervals (Figure S1). In the most extreme cases, the modeled
459 contributions of terrestrial isoGDGTs is higher than the measured isoGDGT
460 abundances (i.e., terrestrial fraction > 1). This is principally seen in iGDGT-2 and
461 GDGT-3, especially when we employ the Paleogene lignite database. This particular
462 assumption clearly overestimates the abundance of terrestrially sourced isoGDGTs in
463 our setting. However, the temporal trends obtained using modern peats, subtropical

464 modern peats and Paleogene lignites are essentially identical and give some indication
465 which isoGDGTs are most likely to be impacted by terrestrial input and across which
466 intervals. Interestingly, this approach also suggests that particularly GDGT-3 is shown
467 to be strongly affected (Figure 5), which qualitatively matches the distributions in the
468 ACEX samples. This is principally because GDGT-3 is the least abundant marine
469 isoGDGT included in our analyses, whereas it is often as abundant as GDGT-1 and 2
470 in terrestrial settings (Fig. 5).

471

472 *5.1.2 Contributions of methanotrophic or methanogenic archaea?*

473 The depositional environment at the study site included ample (export) production,
474 sediment organic matter content, and low oxygen conditions at the sediment-water
475 interface (Sluijs et al., 2006; Stein et al., 2006; Stein, 2007; Sluijs et al., 2008b; Sluijs
476 et al., 2009; März et al., 2010). This may have been suitable for abundant methanogenic
477 and methanotrophic archaea, potentially contributing to the sedimentary isoGDGT
478 assemblage. However, our GDGT-2/Crenarchaeol values (<0.23; Figure 6) are far
479 below values that suggest significant isoGDGT contributions of methanotrophic
480 Euryarchaeota as described by Weijers et al. (2011). MI values (maximum observed
481 0.31) are also generally below proposed cut off values (0.3-0.5, Zhang et al., 2011) that
482 suggest such contributions. Finally, GDGT-0/Crenarchaeol ratios (<1.4) remain below
483 the cut-off value of 2 throughout the section (Figure 6), also making a significant
484 isoGDGT contribution from methanogens highly unlikely (Blaga et al., 2009).
485 Collectively, relative contributions of isoGDGTs from methanogenic and
486 methanotrophic archaea seem low despite the low-oxygen environment, suggesting a
487 relatively high flux of pelagic isoGDGTs.

488

489 *5.1.3 Contributions of deep-dwelling archaea?*

490 Taylor et al. (2013) showed that GDGT-2/GDGT-3 ratios correspond to depth of
491 production, with high values (>5) in deep waters (>1000 m). We record low values (1-
492 4) between ~ 390 and ~ 371.2 mcd (Figure 6), which supports a dominant production in
493 the surface ocean based on the modern calibration data set (Taylor et al., 2013).
494 However, the overlying interval (~ 371 to ~ 368.3 mcd) has much higher (average 7.4)
495 and variable GDGT-2/GDGT-3 values with peak values of 10-14. Such values suggest
496 significant contributions of isoGDGTs produced at water depths of several kilometers
497 according to the analyses by Taylor et al. (2013).

498 However, all paleoenvironmental information generated based on the sediments as well
499 as tectonic reconstructions of Lomonosov Ridge – a strip of continental crust that
500 disconnected from the Siberian margin in the Paleocene - has indicated a neritic setting
501 of the drill site at least up to the middle Eocene (e.g., O'Regan et al., 2008; Sangiorgi
502 et al., 2008; Sluijs et al., 2008a; Sluijs et al., 2009). At ~ 371.2 mcd a drop in BIT index
503 and a change in the palynological assemblages corresponds to an interval of greenish
504 sediment, suggestive of pronounced amounts of glauconite. These changes are
505 consistent with local relative sea level rise, causing a somewhat more distal position
506 relative to the shoreline. However, the sediment remains dominantly siliciclastic and
507 organic terrestrial components, particularly pollen and spores, remain abundant still
508 indicating a shallow setting (Sluijs et al., 2008a; Sluijs et al., 2008b). Increased
509 contributions of isoGDGTs produced at depth would be expected to have caused a
510 systematic cold bias but based on linear regression analysis the large variability in
511 GDGT-2/GDGT-3 ratios is unrelated to the recorded variability in TEX_{86} values. The
512 high GDGT-2/GDGT-3 ratio values can therefore not be explained by contributions of
513 deep dwelling archaea.

514 In a study of the last 160 kyr in the South China Sea, Dong et al. (2019) found that very
515 high GDGT-2/GDGT-3 ratios (~9 but up to 13) correspond with high values in nitrogen
516 isotope ratios, interpreted to reflect low contributions in diazotroph N₂ fixation and
517 enhanced upwelling. In our record, the high GDGT-2/GDGT-3 ratios are associated
518 with normal marine conditions and the dinocyst assemblages are not indicative of
519 upwelling conditions (Sluijs et al., 2009). Unfortunately, the available nitrogen isotope
520 record (Knies et al., 2008) does not cover this interval in sufficient resolution to assess
521 a relation with diazotroph activity. The increase in GDGT-2/GDGT-3 ratio correlates
522 to a strong drop in BIT index values and an increase in normal marine dinocyst species
523 (Sluijs et al., 2009), but a shift to more open marine environment does not explain the
524 high ratio values. As such, the cause of the high GDGT-2/GDGT-3 ratios in this interval
525 remains unclear but we consider it highly unlikely to relate to contributions of deep
526 dwelling Thaumarchaeota.

527

528 *5.1.4 Oxygen concentrations and ammonium oxidation rates*

529 A variety of non-thermal factors can impact TEX₈₆ values, including ammonium and
530 oxygen concentrations and growth phase (Elling et al., 2014; Qin et al., 2014; Hurley
531 et al., 2016). Across the studied interval of the ACEX core, several intervals of seafloor
532 and water column anoxia have been identified based on organic and inorganic proxies,
533 notably during the PETM and ETM2 (Sluijs et al., 2006; Stein et al., 2006; Sluijs et al.,
534 2008b; Sluijs et al., 2009; März et al., 2010).

535 Particularly suspect is an interval of low TEX₈₆ values that marks the middle of the
536 ETM2 interval, directly following a ~4 °C warming at its onset (Sluijs et al., 2009).
537 This interval is also marked by the presence of sulfur-bound isorenieratane (Sluijs et
538 al., 2009), a derivative of isorenieratene. This biomarker is produced by the brown

539 strain of green sulfur bacteria that require light for photosynthesis and free sulfide,
540 indicating euxinic conditions in the (lower) photic zone (Sinninghe Damsté et al.,
541 1993). We also record a concomitant shift in several methane-related indicators,
542 GDGT-2/GDGT-3 ratio values and the Δ RI. A mid-ETM2 cooling signal has not been
543 recorded at other study sites and this interval marks the occurrence of pollen of
544 thermophilic plants such as palms and baobab (Sluijs et al., 2009; Willard et al., 2019).
545 Therefore, the low TEX_{86} values were suggested to reflect thaumarcheotal depth
546 migration to the deeper chemocline due to euxinic conditions (Sluijs et al., 2009),
547 similar to the modern Black Sea (Coolen et al., 2007; Wakeham et al., 2007) and the
548 Mediterranean Sea during sapropel formation (Menzel et al., 2006).
549 More recent work has indicated that the isolated marine Thaumarchaeotal species
550 *Nitrosopumilus maritimus* produces lower TEX_{86} values with higher ammonia
551 oxidation rates (Hurley et al., 2016) and O_2 concentrations (Qin et al., 2015). Although
552 this observation is difficult to extrapolate to the total response of the Thaumarcheotal
553 community in the marine environment on geological time scales, lower O_2 availability
554 should lower oxidation rates leading to higher TEX_{86} values (Qin et al., 2015; Hurley
555 et al., 2016). However, we record a drop in TEX_{86} values with the development of
556 anoxia during ETM2. The nature of the anomalously low cyclization in the ETM2
557 isoGDGT assemblage, which passes all quality tests regarding GDGT distribution
558 (Figure 6), remains therefore elusive.

559

560 5.2 Origin and environmental forcing of brGMGTs

561 The relative abundances of brGMGTs in our samples are surprisingly high. On average,
562 they comprise 25% of the total branched GDGT and GMGT assemblage. The limited
563 literature on modern occurrences implies that both terrestrial and marine sources may

564 have contributed to the brGMGT assemblage. Data from marine sediments (Liu et al.,
565 2012) and the water column (Xie et al., 2014), clearly shows production within the
566 marine realm. Their occurrence in modern peats (Naafs et al., 2018a), lake sediments
567 (Baxter et al., 2019) and Paleogene lignites (Inglis et al., 2019) might also imply
568 transport from land to marine sediments. A soil-derived source is currently
569 unsupported, as they were most often below detection limit in recent studies of
570 geothermally heated soils (De Jonge et al., 2019) and a soil transect from the Peruvian
571 Andes (Kirkels et al., 2020). The brGMGT abundances we record are close to the
572 maximum abundance found in modern peats (Naafs et al., 2018a). However, significant
573 input of peat-derived organic matter into our study site is inconsistent with the low input
574 of peat-derived *Sphagnum* spores (Willard et al., 2019). Alternatively, the high
575 abundance of brGMGTs could also be related to subsurface production in marine
576 sediments. An analogous process was invoked by Naafs et al. (2018a) to explain very
577 high abundance of brGMGTs in an early Paleogene lignite. Collectively, however, we
578 surmise that production in the marine realm may be an important contributor to the
579 brGMGT pool in our setting.

580 Several factors may contribute to the rise in the abundance of brGMGTs relative to
581 brGDGTs across the PETM. Higher relative abundances of brGMGTs in modern peats
582 generally occur at higher mean annual air temperatures (Naafs et al., 2018a) and so this
583 signal could relate to warming during the PETM if their origin at the study site is
584 terrestrial. However, since we consider it likely that a large part of the brGMGTs
585 assemblage is of marine origin, the rise in brGMGT abundance likely relates to the
586 previously recorded (Sluijs et al., 2006; Sluijs et al., 2008b) sea level rise during the
587 PETM at the study site. This is consistent with the increase in marine brGMGT
588 production relative to terrestrial brGDGT supply to the study site (Figure 7b). This is

589 consistent with the inverse correlation between brGMGT abundance and the BIT index
590 (Figure 7b). Lastly, if the production of marine brGMGTs was focused in oxygen
591 minimum zones (Xie et al., 2014), the development of low oxygen conditions in the
592 water column based on several indicators, such as the presence of isorenieratane (Sluijs
593 et al., 2006), might have increased the production of brGMGTs in the water column. It
594 is also possible that all of these factors contributed to the changes in abundance of
595 brGMGTs relative to brGDGTs across the PETM.

596 The brGMGT-I proxy does not produce temperature trends similar to those seen in
597 TEX₈₆ or MBT'_{5me} (Figure 7d). If the majority of the brGMGTs are of marine origin,
598 this indicates that brGMGTs produced in the marine realm do not respond to
599 temperature as was hypothesized based on the African Lake dataset by Baxter et al.
600 (2019).

601 Also the application of the H-MBT_{acyclic} index (equation 7) appeared problematic
602 because, similar to Baxter et al. (2019), we identified several more isomers than Naafs
603 et al. (2018a, who developed this index) detected in their peat samples. It therefore
604 remains unclear which of our peaks should be used to calculate the H-MBT_{acyclic} index
605 values. We therefore show the two plausible options. For the first, we use all peaks with
606 *m/z* 1020, 1034 and 1048 (*H-MBT-all* in Figure 7e) within the expected retention time
607 window. However, based on our chromatography, we consider it more likely that the
608 dominant peaks identified by Naafs et al. (2018a) at *m/z* 1020 and 1034 represent
609 H1020c and H1034b, respectively, and therefore use only those in addition to the single
610 identifiable peak at *m/z* 1048 as a second option (*H-MBT (H1020c, H1034)* in Figure
611 7e. Both options show a clear rise across the PETM, although the HMBT (H1020c,
612 H1034a) shows a larger signal and somewhat better correspondence in absolute values
613 to MBT_{acyclic}, though with more scatter. A close correspondence between MBT_{acyclic}

614 and HMBT has also been found in a lignite that has been assigned to the PETM (Inglis
615 et al., 2019).

616 If the dominant source of the brGMGTs was marine throughout the record, the increase
617 in methylation possibly relates to warming. This would not be unprecedented as marine-
618 produced brGDGTs show an increase in methylation as a function of temperature
619 (Dearing Crampton-Flood et al., 2018). Sollic et al. (2017) also suggest that archaeal-
620 derived isoprenoid GMGTs produced in marine sediments incorporate additional
621 methyl groups at higher sediment temperatures. Water column oxygen concentrations
622 and pH also changed at our site during the PETM, which potentially affected
623 distributions. Extensive evaluation of brGMGT distributions in modern samples is
624 therefore required to assess the proxy potential.

625

626 *5.3 Uncertainty on TEX_{86} -based SST estimates.*

627 *5.3.1 Uncertainty based on calibration dataset*

628 To calculate SSTs, we use 1) the BAYSPAR method (Tierney and Tingley, 2014),
629 which assumes a linear relationship between TEX_{86} and SST, and 2) TEX_{86}^H (Kim et
630 al., 2010), which assumes a non-linear relationship between TEX_{86} and SST.
631 Differences between these calibrations are smaller than the calibration errors (Figure 6)
632 because the TEX_{86} values in the ACEX dataset all fall within the range of the modern
633 core top calibration. Taken together, both indices imply that mean annual SSTs varied
634 between 18 °C and 28 °C in the early Eocene, providing strong evidence for remarkable
635 early Eocene warmth in the Arctic region.

636 The TEX_{86}^H calibration has a calibration error of 2.5 °C (residual mean standard error;
637 RSME) (Kim et al., 2010). The BAYSPAR method yields possible values that range
638 ~6 °C from the most probable value (Figure 6), but these uncertainty estimates are more

639 comparable than is immediately apparent, as this analysis takes a 90% confidence
640 interval compared to the 68% probability of RSME. All of the calibrations and methods
641 to obtain values and uncertainties are based on a modern core-top dataset and thus
642 implicitly include potential confounding factors such as seasonality and depth of
643 production and export. However, there is no (quantitative) constraint on any of these
644 parameters in the calibration data set. This is particularly important for the studied
645 region because it represents a polar endmember of the marine environment with highly
646 seasonal production and export and potentially high seasonality in temperature. In the
647 modern ocean, relations between SST and TEX_{86} in the Arctic and ice-proximal
648 Southern Ocean settings differ from the global ocean. This is attributed to a change in
649 viscoelastic adaptation to temperature at the low end and/or a change in the
650 Thaumarchaeotal community (Kim et al., 2010; Ho et al., 2014; Tierney and Tingley,
651 2014). This may mask potential confounding factors that may be relevant specifically
652 to polar environments. This is important here, where the polar regions were ice free and
653 the functioning of physical, chemical and biological ocean systems were fundamentally
654 different from present day. This uncertainty is not accounted for using traditional
655 regression analyses or Bayesian techniques and quantification of uncertainty in non-
656 analogue climates remains extremely difficult.

657

658 5.3.2 Constraints from independent proxy data

659 Independent proxy data may provide additional constraints. The appearance of the
660 dinoflagellate cyst genus *Apectodinium* during the PETM and ETM2 in the Arctic basin
661 (Sluijs et al., 2006; Sluijs et al., 2009; Harding et al., 2011) provide qualitative support
662 for pronounced warming and apparent subtropical conditions. Recent efforts to quantify
663 the paleoecological affinities of this now extinct genus have suggested a required

664 minimum temperature of $\sim 20^{\circ}\text{C}$ (Frieling et al., 2014; Frieling and Sluijs, 2018).
665 Although this value is partly based on TEX_{86} data from the ACEX cores, it is supported
666 by data from an epicontinental site in Siberia (Frieling et al., 2014).
667 A second line of independent proxy evidence includes vegetation reconstructions. As
668 indicated above, the TEX_{86} results are qualitatively consistent with the ample evidence
669 for thermophilic plants and animals in the Arctic (e.g., Heer, 1869; Schweitzer, 1980;
670 Greenwood and Wing, 1995; Uhl et al., 2007; Suan et al., 2017). Particularly valuable
671 are minimum winter temperature tolerances for specific plant species. Palynological
672 analyses have indicated the presence of palm and baobab pollen within the PETM and
673 ETM2 intervals in the ACEX cores (Sluijs et al., 2009; Willard et al., 2019). Modern
674 palms are unable to tolerate sustained intervals of frost and sexual reproduction is
675 limited to regions where the coldest month mean temperature (CMMT) is significantly
676 above freezing (Van der Burgh, 1984; Greenwood and Wing, 1995). This threshold was
677 recently quantified to be $\geq 5.2^{\circ}\text{C}$ (Reichgelt et al., 2018). The presence of baobab
678 within the PETM interval and ETM2 also indicate mean winter air temperatures of at
679 least 6°C (Willard et al., 2019). Importantly, these plants were not encountered in the
680 intervals outside the PETM and ETM2, suggesting background coldest month mean air
681 temperatures were potentially too low ($<6^{\circ}\text{C}$) to support megathermal vegetation.
682 Pollen of palms and *Avicennia* mangroves were recently identified in time-equivalent
683 sections in Arctic Siberia (Suan et al., 2017). Although the details of stratigraphic
684 framework for these records may be somewhat problematic, these findings indicate
685 elevated CMMT estimates on land ($>5.5^{\circ}\text{C}$) and in the surface ocean ($>13^{\circ}\text{C}$) during
686 the late Paleocene and early Eocene (Suan et al., 2017).
687 Apparently conflicting evidence comes from the occurrence of glendonites and erratics
688 in specific stratigraphic levels in Paleocene and Eocene strata in Spitsbergen,

689 interpreted to reflect ‘cold snaps’ in climate (Spielhagen and Tripati, 2009). Some of
690 these stratigraphic levels are very close to (or even potentially within) the PETM,
691 considering the local stratigraphic level of the PETM (Cui et al., 2011; Harding et al.,
692 2011). However, glendonites and erratics have not been found at the exact same
693 stratigraphic levels as thermophilic biota (Spielhagen and Tripati, 2009). The formation
694 and stability of ikaite (the precursor mineral of the diagenetic glendonites) in
695 Spitsbergen was dependent on relatively low temperature, arguably persistent near-
696 freezing sea water temperatures in the sediment (Spielhagen and Tripati, 2009).
697 However, glendonite occurrences in other settings (e.g. Mesozoic sediments in mid-
698 latitude regions, Teichert and Luppold, 2013) have recently also been linked to methane
699 seeps (Morales et al., 2017). Therefore, the specific temperature constraints implied by
700 glendonites under such conditions are subject of debate. Future work should apply
701 temperature reconstructions based on the geochemical composition of the glendonites,
702 and biomarkers or biota on corresponding strata to assess whether glendonite
703 occurrence is related to colder climates.

704 The estimate on seasonal minima provides an important constraint on Arctic
705 climatology during the PETM and ETM2. Most likely, the palms and baobabs grew
706 close to the shore, where the relative heat of the ocean kept atmospheric temperatures
707 relatively high during the winter. If minimum winter SSTs were in the range of the SST
708 reconstructions based on the nearby *Avicennia* mangrove pollen (Suan et al., 2017),
709 which for open ocean settings would perhaps amount to \sim 10 °C, then summer SST must
710 have soared to at least 30 °C in summer if TEX₈₆-based SST reconstructions of \sim 20 °C
711 truly reflects the annual mean. It would imply an SST seasonality of \sim 20 °C, much
712 higher than any modern open marine setting. In the present day Arctic Ocean, heat is
713 seasonally stored and released in sea ice melting and freezing, and sea ice cover

714 insulates the ocean and reflects much sunlight, resulting in a seasonal cycle of not more
715 than 1.5 °C, even in ice-free regions (Chepurin and Carton, 2012). However, coupled
716 model simulations have indicated that the future loss of sea ice will greatly enhance the
717 seasonal SST range to up to 10 °C in 2300 given unabated CO₂ emissions (Carton et
718 al., 2015). With year-round snow and ice-free conditions, even stronger summer
719 stratification during the Eocene due to higher greenhouse gas concentrations and fresh-
720 water supply through an enhanced hydrological cycle (Pierrehumbert, 2002;
721 Carmichael et al., 2017), a near-shore 20 °C seasonal cycle in Arctic Ocean SST may
722 not be unrealistic, although it remains inconsistent with current-generation fully
723 coupled, relatively low resolution, model simulations (e.g., Frieling et al., 2017).
724 Constraints from the total pollen assemblages in the ACEX cores based on a nearest
725 living relative approach suggest Arctic mean annual temperatures on land of 13-18 °C,
726 and summer temperatures significantly exceeding 20 °C during the PETM and ETM2
727 (Willard et al., 2019). Although these estimates come with much larger uncertainty than
728 winter temperatures and may suffer from the non-analogous setting, they are generally
729 lower than our TEX₈₆ values. The brGDGT-based paleothermometer MBT'_{5me} (De
730 Jonge et al., 2014) also indicates lower mean annual air temperatures than reported from
731 TEX₈₆ (Willard et al., 2019, Figure 7). These data, derived from the same UHPLC/MS
732 analyses as the isoGDGT data presented here, indicate mean annual air temperatures
733 averaging ~18 °C during the PETM, with a residual mean calibration error of 4.8 °C.
734 This value is ~7 °C lower than earlier estimates based on a slightly different method,
735 analytical procedure and a smaller modern calibration dataset (Weijers et al., 2007a).

736

737 *5.4 State of constraints on Paleocene-Eocene Arctic temperatures*

738 To unlock the unique premise of Eocene climates for testing the skill of current-
739 generation fully coupled climate models under high greenhouse gas forcing, proxy data
740 and models are ideally approached separately. Among the most important implications
741 of the Arctic temperature estimates are reconstructions of the meridional temperature
742 gradients. Importantly, not a single simulation using an IPCC-class model of early
743 Paleogene climate has produced Arctic annual mean sea surface temperatures close to
744 the ACEX TEX₈₆-based reconstructions without unrealistically high tropical SSTs
745 (Lunt et al., 2012). Recent simulations using the Community Earth System Model
746 (CESM) versions 1 (Frieling et al., 2017; Cramwinckel et al., 2018) and 1.2 (Zhu et al.,
747 2019) using Eocene boundary conditions produced climates that correspond to SST
748 reconstructions in many ocean regions based on several proxies, but still produced
749 cooler mean annual SSTs for the Arctic Ocean than suggested by TEX₈₆ (Frieling et al.,
750 2017; Cramwinckel et al., 2018; Zhu et al., 2019). TEX₈₆ also indicates SSTs higher
751 than in these model simulations at several sites along the Antarctic margin (Bijl et al.,
752 2009; Bijl et al., 2013). The question thus remains if the conversion of TEX₈₆ values
753 towards mean annual SST using any modern core-top calibration for high latitude
754 Paleogene locations is valid, or if the climate models still significantly underestimate
755 polar temperatures. Certainly, if interpreted as mean annual SST, TEX₈₆-based
756 estimates are high compared to the few available additional estimates, notably based on
757 vegetation, but the latter also suffer from similar uncertainties (e.g., Hollis et al., 2019).
758 A few biases might lead to underestimates of meridional temperature gradients as
759 indicated from TEX₈₆. First, the flat Eocene temperature gradient implied by TEX₈₆
760 was suggested to result from erroneously calibrating the proxy to SST rather than to the
761 temperature of the subsurface (Ho and Laepple, 2016). The rationale is that the

762 meridional temperature gradient is smaller in deeper waters than it is in the surface.
763 However, the idea was contested for multiple reasons, including the fact that sediments
764 at most Eocene study sites, such as the ACEX site, were deposited at a depth of less
765 than 200m, making the application of a deep subsurface (>1000m) calibration
766 inappropriate (Tierney et al., 2017). Moreover, recent analyses have indicated that the
767 TEX₈₆ signal dominantly reflects temperature of top 200 m of the water column (Zhang
768 and Liu, 2018).

769 Secondly, as suggested previously (Sluijs et al., 2006), if TEX₈₆ were biased towards
770 any season in the non-analogue Arctic Ocean, it would be the summer, the dominant
771 season of organic matter export towards the seafloor through fecal pelleting or marine
772 snow aggregates. Vegetation suggests very high winter continental coldest month mean
773 air temperatures of at least 6-8 °C (Sluijs et al., 2009; Suan et al., 2017; Willard et al.,
774 2019), coastal coldest month mean SSTs of >13 °C (Suan et al., 2017), and terrestrial
775 mean annual and warmest month mean temperature on land of 13-21 °C and >20°C,
776 respectively (Suan et al., 2017; Willard et al., 2019) (see section 5.3.2). These estimates
777 are closer to the most recent model simulations and lower than the existing TEX₈₆ (e.g.,
778 Frielings et al., 2017; Zhu et al., 2019). If TEX₈₆-implied SST of ~25 °C is skewed
779 towards a summer estimate, this would decrease the model-data bias regarding the
780 meridional temperature gradient estimates. Given the current uncertainties in the use of
781 TEX₈₆ for the non-analogue Arctic Ocean, we however cannot independently constrain
782 this.

783

784 **6. Conclusions**

785 We analyzed isoGDGT and brGMGT (H-shaped brGDGT) distributions in sediments
786 recovered from the Paleocene-Eocene Thermal Maximum (PETM; ~56 Ma) to Eocene

787 Thermal Maximum 2 (ETM2; ~54 Ma) interval on Lomonosov Ridge, Arctic Ocean
788 using state-of-the-art analytical procedures, compare them to the original dataset (Sluijs
789 et al., 2006; Sluijs et al., 2009) and interpret the results following the currently available
790 TEX₈₆ proxy constraints.

791 Although contributions of isoGDGTs from land complicate TEX₈₆ paleothermometry
792 in some stratigraphic intervals, temperature was the dominant variable controlling
793 TEX₈₆ values. Background early Eocene SSTs exceed ~20 °C and peak warmth
794 occurred during the PETM and ETM2. However, uncertainty estimates of these SSTs
795 based on the non-analogue modern ocean, remains complex. Temperature constraints
796 from terrestrial vegetation support remarkable warmth in the study section and
797 elsewhere in the Arctic basin, notably coldest month mean temperatures around 10 °C
798 at least within the PETM and ETM2. If TEX₈₆-derived SSTs of ~20 °C truly represent
799 mean annual SSTs, the seasonal range of Arctic SST might have been in the order of
800 20 °C. If SST estimates are entirely skewed towards the summer season, seasonal
801 ranges in the order of 10 °C may be considered comparable to those simulated in future
802 ice-free Arctic Ocean scenarios.

803 We find abundant brGMGTs, which appear predominantly produced in the marine
804 realm at the study site. Their abundance increases during the PETM, likely due to sea
805 level rise and perhaps due to warming and a drop in seawater oxygen concentrations.
806 Although speculative, an increase in brGMGT methylation during the PETM may be a
807 function of temperature, but a relation between brGMGT distribution and
808 environmental parameters including temperature is yet to be confirmed.

809

810 **6. Data Availability**

811 All data is provided in the Supplement Table and will be included in the PANGAEA
812 database upon publication of this paper.

813

814 **7. Sample Availability**

815 Requests for materials can be addressed to A.Sluijs@uu.nl

816

817 **8. Author Contributions**

818 AS initiated the study, KGJN generated the data, JF modeled terrestrial contributions
819 of isoGDGTs based on published information and the new Crenarchaeol data of the
820 modern peat dataset, which was contributed by GNI. All authors contributed to the
821 interpretation of the data and AS wrote the paper with input from all authors.

822

823 **9. Competing Interests**

824 The authors declare no competing interests

825

826 **10. Acknowledgments**

827 We thank the ACEX scientific party for collaborations over the past 16 years, the
828 International Ocean Discovery Program (IODP) for access to ACEX samples and data,
829 and the Dutch Research Council (NWO) for their continued support to IODP. We thank
830 Linda van Roij for analytical support.

831 This research was funded by European Research Council Consolidator Grant 771497
832 awarded to AS and the Netherlands Earth System Science Centre, funded through a
833 Gravitation Grant by the Netherlands Ministry of Education, Culture and Science and
834 NWO. GNI acknowledges a GCRF Royal Society Dorothy Hodgkin Fellowship and

835 thanks David Naafs for providing the original chromatograms published in Naafs et al.
836 (2018b).

837

838 **11. References**

839 Backman, J., Moran, K., McInroy, D. B., Mayer, L. A., and Expedition-302-Scientists:
840 Proceedings of the Integrated Ocean Drilling Program, 302, Integrated Ocean
841 Drilling Program Management International, Inc., Edinburgh, 2006.

842 Baxter, A. J., Hopmans, E. C., Russell, J. M., and Sinninghe Damsté, J. S.: Bacterial
843 GMGTs in East African lake sediments: Their potential as palaeotemperature
844 indicators, *Geochim Cosmochim Ac*, 259, 155-169,
845 <https://doi.org/10.1016/j.gca.2019.05.039>, 2019.

846 Berry, E. W.: A Possible Explanation of Upper Eocene Climates, *Proceedings of the*
847 *American Philosophical Society*, 61, 1-14, 1922.

848 Besseling, M. A., Hopmans, E. C., Bale, N. J., Schouten, S., Damsté, J. S. S., and
849 Villanueva, L.: The absence of intact polar lipid-derived GDGTs in marine waters
850 dominated by Marine Group II: Implications for lipid biosynthesis in Archaea,
851 *Scientific Reports*, 10, 294, 10.1038/s41598-019-57035-0, 2020.

852 Bijl, P. K., Schouten, S., Sluijs, A., Reichart, G.-J., Zachos, J. C., and Brinkhuis, H.:
853 Early Palaeogene temperature evolution of the southwest Pacific Ocean, *Nature*,
854 461, 776-779, 2009.

855 Bijl, P. K., Bendle, J. A. P., Bohaty, S. M., Pross, J., Schouten, S., Tauxe, L., Stickley,
856 C. E., McKay, R. M., Rohl, U., Olney, M., Sluijs, A., Escutia, C., Brinkhuis, H.,
857 and the Expedition 318 Scientists: Eocene cooling linked to early flow across the
858 Tasmanian Gateway, *Proceedings of the National Academy of Sciences*, 110,
859 9645-9650, 10.1073/pnas.1220872110, 2013.

860 Blaga, C. I., Reichart, G.-J., Heiri, O., and Sinninghe Damsté, J. S.: Tetraether
861 membrane lipid distributions in water-column particulate matter and sediments: a
862 study of 47 European lakes along a north–south transect, *Journal of*
863 *Paleolimnology*, 41, 523-540, 10.1007/s10933-008-9242-2, 2009.

864 Carton, J. A., Ding, Y., and Arrigo, K. R.: The seasonal cycle of the Arctic Ocean under
865 climate change, *Geophysical Research Letters*, 42, 7681-7686,
866 doi:10.1002/2015GL064514, 2015.

867 Chepurin, G. A., and Carton, J. A.: Subarctic and Arctic sea surface temperature and its
868 relation to ocean heat content 1982–2010, *Journal of Geophysical Research: Oceans*, 117, doi:10.1029/2011JC007770, 2012.

869 Coolen, M. J. L., Abbas, B., Bleijswijk, J. v., Hopmans, E. C., Kuypers, M. M. M.,
870 Wakeham, S. G., and Damsté, J. S. S.: Putative ammonia-oxidizing Crenarchaeota
871 in suboxic waters of the Black Sea: a basin-wide ecological study using 16S
872 ribosomal and functional genes and membrane lipids, *Environ Microbiol*, 9, 1001-
873 1016, 2007.

874 Cramwinckel, M. J., Huber, M., Kocken, I. J., Agnini, C., Bijl, P. K., Bohaty, S. M.,
875 Frieling, J., Goldner, A., Hilgen, F. J., Kip, E. L., Peterse, F., van der Ploeg, R.,
876 Röhl, U., Schouten, S., and Sluijs, A.: Synchronous tropical and polar temperature
877 evolution in the Eocene, *Nature*, 559, 382-386, 10.1038/s41586-018-0272-2, 2018.

878 Cui, Y., Kump, L. R., Ridgwell, A. J., Charles, A. J., Junium, C. K., Diefendorf, A. F.,
879 Freeman, K. H., Urban, N. M., and Harding, I. C.: Slow release of fossil carbon

881 during the Palaeocene-Eocene Thermal Maximum, *Nature Geoscience*, 4, 481-485,
 882 2011.

883 Dawson, M. R., West, R. M., Langston Jr, W., and Hutchison, J. H.: Paleogene
 884 terrestrial vertebrates: Northernmost occurrence, Ellesmere Island, Canada,
 885 *Science*, 192, 781-782, 1976.

886 De Jonge, C., Hopmans, E. C., Zell, C. I., Kim, J.-H., Schouten, S., and Sinninghe
 887 Damsté, J. S.: Occurrence and abundance of 6-methyl branched glycerol dialkyl
 888 glycerol tetraethers in soils: Implications for palaeoclimate reconstruction,
 889 *Geochim Cosmochim Ac*, 141, 97-112, <https://doi.org/10.1016/j.gca.2014.06.013>,
 890 2014.

891 De Jonge, C., Radujković, D., Sigurdsson, B. D., Weedon, J. T., Janssens, I., and
 892 Peterse, F.: Lipid biomarker temperature proxy responds to abrupt shift in the
 893 bacterial community composition in geothermally heated soils, *Org Geochem*, 137,
 894 103897, <https://doi.org/10.1016/j.orggeochem.2019.07.006>, 2019.

895 De Rosa, M., Esposito, E., Gambacorta, A., Nicolaus, B., and Bu'Lock, J. D.: Effects
 896 of temperature on ether lipid composition of *Caldariella acidiphila*,
 897 *Phytochemistry*, 19, 827-831, [https://doi.org/10.1016/0031-9422\(80\)85120-X](https://doi.org/10.1016/0031-9422(80)85120-X),
 898 1980.

899 Dearing Crampton-Flood, E., Peterse, F., Munsterman, D., and Sinninghe Damsté, J.
 900 S.: Using tetraether lipids archived in North Sea Basin sediments to extract North
 901 Western European Pliocene continental air temperatures, *Earth and Planetary
 902 Science Letters*, 490, 193-205, <https://doi.org/10.1016/j.epsl.2018.03.030>, 2018.

903 Dong, L., Li, Z., and Jia, G.: Archaeal ammonia oxidation plays a part in late
 904 Quaternary nitrogen cycling in the South China Sea, *Earth and Planetary Science
 905 Letters*, 509, 38-46, <https://doi.org/10.1016/j.epsl.2018.12.023>, 2019.

906 Douglas, P. M. J., Affek, H. P., Ivany, L. C., Houben, A. J. P., Sijp, W. P., Sluijs, A.,
 907 Schouten, S., and Pagani, M.: Pronounced zonal heterogeneity in Eocene southern
 908 high-latitude sea surface temperatures, *Proceedings of the National Academy of
 909 Sciences of the United States of America*, 111, 6582-6587, 2014.

910 Eberle, J. J., and Greenwood, D. R.: Life at the top of the greenhouse Eocene world—
 911 A review of the Eocene flora and vertebrate fauna from Canada's High Arctic,
 912 *GSA Bulletin*, 124, 3-23, 10.1130/B30571.1, 2012.

913 Elling, F. J., Könneke, M., Lipp, J. S., Becker, K. W., Gagen, E. J., and Hinrichs, K.-U.: Effects of growth phase on the membrane lipid composition of the
 914 thaumarchaeon *Nitrosopumilus maritimus* and their implications for archaeal lipid
 915 distributions in the marine environment, *Geochim Cosmochim Ac*, 141, 579-597,
 916 <https://doi.org/10.1016/j.gca.2014.07.005>, 2014.

917 Elling, F. J., Könneke, M., Mußmann, M., Greve, A., and Hinrichs, K.-U.: Influence of
 918 temperature, pH, and salinity on membrane lipid composition and TEX86 of
 919 marine planktonic thaumarchaeal isolates, *Geochim Cosmochim Ac*, 171, 238-255,
 920 <https://doi.org/10.1016/j.gca.2015.09.004>, 2015.

921 Estes, R., and Hutchinson, J. H.: Eocene Lower Vertebrates from Ellesmere Island,
 922 Canadian Arctic Archipelago, *Palaeogeography, Palaeoclimatology,
 923 Palaeoecology*, 30, 325-347, 1980.

924 Evans, D., Sagoo, N., Renema, W., Cotton, L. J., Müller, W., Todd, J. A., Saraswati, P.
 925 K., Stassen, P., Ziegler, M., Pearson, P. N., Valdes, P. J., and Affek, H. P.: Eocene
 926 greenhouse climate revealed by coupled clumped isotope-Mg/Ca thermometry,
 927 *Proceedings of the National Academy of Sciences*, 115, 1174-1179,
 928 [10.1073/pnas.1714744115](https://doi.org/10.1073/pnas.1714744115), 2018.

929

930 Frieling, J., Iakovleva, A. I., Reichart, G. J., Aleksandrova, G. N., Gnibidenko, Z. N.,
 931 Schouten, S., and Sluijs, A.: Paleocene-Eocene warming and biotic response in the
 932 epicontinental West Siberian Sea, *Geology*, 42, 767-770, 2014.

933 Frieling, J., Gebhardt, H., Huber, M., Adekeye, O. A., Akande, S. O., Reichart, G.-J.,
 934 Middelburg, J. J., Schouten, S., and Sluijs, A.: Extreme warmth and heat-stressed
 935 plankton in the tropics during the Paleocene-Eocene Thermal Maximum, *Science
 936 Advances*, 3, e1600891, 10.1126/sciadv.1600891, 2017.

937 Frieling, J., and Sluijs, A.: Towards quantitative environmental reconstructions from
 938 ancient non-analogue microfossil assemblages: Ecological preferences of
 939 Paleocene – Eocene dinoflagellates, *Earth-Science Reviews*, 185, 956-973,
 940 <https://doi.org/10.1016/j.earscirev.2018.08.014>, 2018.

941 Greenwood, D. R., and Wing, S. L.: Eocene continental climates and latitudinal
 942 temperature gradients, *Geology*, 23, 1044-1048, 1995.

943 Greenwood, D. R., Basinger, J. F., and Smith, R. Y.: How wet was the Arctic Eocene
 944 rain forest? Estimates of precipitation from Paleogene Arctic macrofloras,
 945 *Geology*, 38, 15-18, 10.1130/G30218.1, 2010.

946 Harding, I. C., Charles, A. J., Marshall, J. E. A., Pälike, H., Roberts, A. P., Wilson, P.
 947 A., Jarvis, E., Thorne, R., Morris, E., Moremon, R., Pearce, R. B., and Akbari, S.:
 948 Sea-level and salinity fluctuations during the Paleocene-Eocene thermal maximum
 949 in Arctic Spitsbergen, *Earth and Planetary Science Letters*, 303, 97-107, 2011.

950 Heer, O.: *Flora fossilis Arctica*, Kongliga Svenska Wetenskaps Academiens
 951 Handlingar, 4, Stockholm, Sweden, 41 pp., 1869.

952 Ho, S. L., Mollenhauer, G., Fietz, S., Martínez-Garcia, A., Lamy, F., Rueda, G.,
 953 Schipper, K., Méheust, M., Rosell-Melé, A., Stein, R., and Tiedemann, R.:
 954 Appraisal of TEX86 and TEX86L thermometries in subpolar and polar regions,
 955 *Geochim Cosmochim Ac*, 131, 213-226,
 956 <https://doi.org/10.1016/j.gca.2014.01.001>, 2014.

957 Ho, S. L., and Laepple, T.: Flat meridional temperature gradient in the early Eocene in
 958 the subsurface rather than surface ocean, *Nature Geoscience*, 9, 606-610,
 959 [10.1038/ngeo2763](https://doi.org/10.1038/ngeo2763).[#supplementary-information](http://www.nature.com/ngeo/journal/v9/n8/abs/ngeo2763.html), 2016.

960 Hollis, C. J., Dunkley Jones, T., Anagnostou, E., Bijl, P. K., Cramwinckel, M. J., Cui,
 961 Y., Dickens, G. R., Edgar, K. M., Eley, Y., Evans, D., Foster, G. L., Frieling, J.,
 962 Inglis, G. N., Kennedy, E. M., Kozdon, R., Lauretano, V., Lear, C. H., Littler, K.,
 963 Lourens, L., Meckler, A. N., Naafs, B. D. A., Pälike, H., Pancost, R. D., Pearson,
 964 P. N., Röhl, U., Royer, D. L., Salzmann, U., Schubert, B. A., Seebeck, H., Sluijs,
 965 A., Speijer, R. P., Stassen, P., Tierney, J., Tripati, A., Wade, B., Westerhold, T.,
 966 Witkowski, C., Zachos, J. C., Zhang, Y. G., Huber, M., and Lunt, D. J.: The
 967 DeepMIP contribution to PMIP4: methodologies for selection, compilation and
 968 analysis of latest Paleocene and early Eocene climate proxy data, incorporating
 969 version 0.1 of the DeepMIP database, *Geosci. Model Dev.*, 12, 3149-3206,
 970 [10.5194/gmd-12-3149-2019](https://doi.org/10.5194/gmd-12-3149-2019), 2019.

971 Hopmans, E. C., Schouten, S., Pancost, R. D., Meer, M. T. J. v. d., and Damsté, J. S.
 972 S.: Analysis of intact tetraether lipids in archaeal cell material and sediments by
 973 high performance liquid chromatography/atmospheric pressure chemical
 974 ionization mass spectrometry, *Rapid Communications in Mass Spectrometry*, 14,
 975 585-589, 2000.

976 Hopmans, E. C., Weijers, J. W. H., Schefuß, E., Herfort, L., Sinninghe Damsté, J. S.,
 977 and Schouten, S.: A novel proxy for terrestrial organic matter in sediments based

979 on branched and isoprenoid tetraether lipids, *Earth and Planetary Science Letters*,
980 224, 107-116, 2004.

981 Hopmans, E. C., Schouten, S., and Sinninghe Damsté, J. S.: The effect of improved
982 chromatography on GDGT-based palaeoproxies, *Org Geochem*, 93, 1-6,
983 <https://doi.org/10.1016/j.orggeochem.2015.12.006>, 2016.

984 Hurley, S. J., Elling, F. J., Könneke, M., Buchwald, C., Wankel, S. D., Santoro, A. E.,
985 Lipp, J. S., Hinrichs, K.-U., and Pearson, A.: Influence of ammonia oxidation rate
986 on thaumarchaeal lipid composition and the TEX₈₆ temperature proxy, *Proceedings
987 of the National Academy of Sciences*, 113, 7762-7767, 10.1073/pnas.1518534113,
988 2016.

989 Inglis, G. N., Farnsworth, A., Lunt, D., Foster, G. L., Hollis, C. J., Pagani, M., Jardine,
990 P. E., Pearson, P. N., Markwick, P., Galsworthy, A. M. J., Raynham, L., Taylor,
991 K. W. R., and Pancost, R. D.: Descent toward the Icehouse: Eocene sea surface
992 cooling inferred from GDGT distributions, *Paleoceanography*, 30, 1000-1020,
993 10.1002/2014PA002723, 2015.

994 Inglis, G. N., Farnsworth, A., Collinson, M. E., Carmichael, M. J., Naafs, B. D. A.,
995 Lunt, D. J., Valdes, P. J., and Pancost, R. D.: Terrestrial environmental change
996 across the onset of the PETM and the associated impact on biomarker proxies: A
997 cautionary tale, *Global and Planetary Change*, 181, 102991,
998 <https://doi.org/10.1016/j.gloplacha.2019.102991>, 2019.

999 Jaeschke, A., Jørgensen, S. L., Bernasconi, S. M., Pedersen, R. B., Thorseth, I. H., and
1000 Früh-Green, G. L.: Microbial diversity of Loki's Castle black smokers at the Arctic
1001 Mid-Ocean Ridge, *Geobiology*, 10, 548-561, 10.1111/gbi.12009, 2012

1002 Karner, M. B., DeLong, E. F., and Karl, D. M.: Archaeal dominance in the mesopelagic
1003 zone of the Pacific Ocean, *Nature*, 409, 507-510, 10.1038/35054051, 2001.

1004 Kim, J.-H., Schouten, S., Hopmans, E. C., Donner, B., and Sinninghe Damste, J. S.:
1005 Global sediment core-top calibration of the TEX86 paleothermometer in the ocean,
1006 *Geochim Cosmochim Ac*, 72, 1154-1173, 2008.

1007 Kim, J.-H., van der Meer, J., Schouten, S., Helmke, P., Willmott, V., Sangiorgi, F.,
1008 Koç, N., Hopmans, E. C., and Sinnenhe Damsté, J. S.: New indices and
1009 calibrations derived from the distribution of crenarchaeal isoprenoid tetraether
1010 lipids: Implications for past sea surface temperature reconstructions, *Geochim
1011 Cosmochim Ac*, 74, 4639-4654, 2010.

1012 Kim, J.-H., Schouten, S., Rodrigo-Gámiz, M., Rampen, S., Marino, G., Huguet, C.,
1013 Helmke, P., Buscail, R., Hopmans, E. C., Pross, J., Sangiorgi, F., Middelburg, J.
1014 B. M., and Sinnenhe Damsté, J. S.: Influence of deep-water derived isoprenoid
1015 tetraether lipids on the paleothermometer in the Mediterranean Sea, *Geochim
1016 Cosmochim Ac*, 150, 125-141, <http://dx.doi.org/10.1016/j.gca.2014.11.017>, 2015.

1017 Kirkels, F. M. S. A., Ponton, C., Galy, V., West, A. J., Feakins, S. J., and Peterse, F.:
1018 From Andes to Amazon: Assessing Branched Tetraether Lipids as Tracers for Soil
1019 Organic Carbon in the Madre de Dios River System, *Journal of Geophysical
1020 Research: Biogeosciences*, 125, e2019JG005270, 10.1029/2019jg005270, 2020.

1021 Knies, J., Mann, U., Popp, B. N., Stein, R., and Brumsack, H.-J.: Surface water
1022 productivity and paleoceanographic implications in the Cenozoic Arctic Ocean,
1023 *Paleoceanography*, 23, PA1S16, 10.1029/2007pa001455, 2008.

1024 Könneke, M., Bernhard, A. E., de la Torre, J. R., Walker, C. B., Waterbury, J. B., and
1025 Stahl, D. A.: Isolation of an autotrophic ammonia-oxidizing marine archaeon,
1026 *Nature*, 437, 543-546, 10.1038/nature03911, 2005.

1027 Liu, X.-L., Summons, R. E., and Hinrichs, K.-U.: Extending the known range of
1028 glycerol ether lipids in the environment: structural assignments based on tandem

1029 mass spectral fragmentation patterns, *Rapid Communications in Mass*
1030 *Spectrometry*, 26, 2295-2302, 10.1002/rcm.6355, 2012.

1031 Liu, Z., Pagani, M., Zinniker, D., DeConto, R., Huber, M., Brinkhuis, H., Shah, S. R.,
1032 Leckie, R. M., and Pearson, A.: Global Cooling During the Eocene-Oligocene
1033 Climate Transition, *Science*, 323, 1187-1190, 10.1126/science.1166368, 2009.

1034 Lunt, D. J., Jones, T. D., Heinemann, M., Huber, M., LeGrande, A., Winguth, A.,
1035 Loptson, C., Marotzke, J., Roberts, C. D., Tindall, J., Valdes, P., and Winguth, C.:
1036 A model-data comparison for a multi-model ensemble of early Eocene
1037 atmosphere-ocean simulations: EoMIP, *Climate of the Past*, 8, 1717-1736, 2012.

1038 März, C., Schnetger, B., and Brumsack, H. J.: Paleoenvironmental implications of
1039 Cenozoic sediments from the central Arctic Ocean (IODP Expedition 302) using
1040 inorganic geochemistry, *Paleoceanography*, 25, PA3206, 10.1029/2009pa001860,
1041 2010.

1042 Menzel, D., Hopmans, E. C., Schouten, S., and Sinninghe Damsté, J. S.: Membrane
1043 tetraether lipids of planktonic Crenarchaeota in Pliocene sapropels of the eastern
1044 Mediterranean Sea, *Palaeogeography, Palaeoclimatology, Palaeoecology*, 239, 1-
1045 15, 2006.

1046 Mollenhauer, G., Basse, A., Kim, J.-H., Sinninghe Damsté, J. S., and Fischer, G.: A
1047 four-year record of UK' 37- and TEX86-derived sea surface temperature
1048 estimates from sinking particles in the filamentous upwelling region off Cape
1049 Blanc, Mauritania, *Deep Sea Research Part I: Oceanographic Research Papers*, 97,
1050 67-79, <https://doi.org/10.1016/j.dsr.2014.11.015>, 2015.

1051 Morales, C., Rogov, M., Wierzbowski, H., Ershova, V., Suan, G., Adatte, T., Föllmi,
1052 K. B., Tegelaar, E., Reichart, G.-J., de Lange, G. J., Middelburg, J. J., and van de
1053 Schootbrugge, B.: Glendonites track methane seepage in Mesozoic polar seas,
1054 *Geology*, 45, 503-506, 10.1130/g38967.1, 2017.

1055 Müller, R. D., Cannon, J., Qin, X., Watson, R. J., Gurnis, M., Williams, S.,
1056 Pfaffelmoser, T., Seton, M., Russell, S. H. J., and Zahirovic, S.: GPlates: Building
1057 a Virtual Earth Through Deep Time, *Geochemistry, Geophysics, Geosystems*, 19,
1058 2243-2261, 10.1029/2018gc007584, 2018

1059 Naafs, B. D. A., Inglis, G. N., Zheng, Y., Amesbury, M. J., Biester, H., Bindler, R.,
1060 Blewett, J., Burrows, M. A., del Castillo Torres, D., Chambers, F. M., Cohen, A.
1061 D., Evershed, R. P., Feakins, S. J., Gałka, M., Gallego-Sala, A., Gandois, L., Gray,
1062 D. M., Hatcher, P. G., Honorio Coronado, E. N., Hughes, P. D. M., Huguet, A.,
1063 Könönen, M., Laggoun-Défarge, F., Lähteenoja, O., Lamentowicz, M., Marchant,
1064 R., McClymont, E., Pontevedra-Pombal, X., Ponton, C., Pourmand, A., Rizzuti, A.
1065 M., Rochefort, L., Schellekens, J., De Vleeschouwer, F., and Pancost, R. D.:
1066 Introducing global peat-specific temperature and pH calibrations based on
1067 brGDGT bacterial lipids, *Geochim Cosmochim Ac*, 208, 285-301,
1068 <https://doi.org/10.1016/j.gca.2017.01.038>, 2017.

1069 Naafs, B. D. A., McCormick, D., Inglis, G. N., and Pancost, R. D.: Archaeal and
1070 bacterial H-GDGTS are abundant in peat and their relative abundance is positively
1071 correlated with temperature, *Geochim Cosmochim Ac*, 227, 156-170,
1072 <https://doi.org/10.1016/j.gca.2018.02.025>, 2018a.

1073 Naafs, B. D. A., Rohrsen, M., Inglis, G. N., Lähteenoja, O., Feakins, S. J., Collinson,
1074 M. E., Kennedy, E. M., Singh, P. K., Singh, M. P., Lunt, D. J., and Pancost, R. D.:
1075 High temperatures in the terrestrial mid-latitudes during the early Palaeogene,
1076 *Nature Geoscience*, 11, 766-771, 10.1038/s41561-018-0199-0, 2018b.

1077 O'Brien, C. L., Robinson, S. A., Pancost, R. D., Sinninghe Damsté, J. S., Schouten, S.,
1078 Lunt, D. J., Alsenz, H., Bornemann, A., Bottini, C., Brassell, S. C., Farnsworth, A.,

1079 Forster, A., Huber, B. T., Inglis, G. N., Jenkyns, H. C., Linnert, C., Littler, K.,
1080 Markwick, P., McAnena, A., Mutterlose, J., Naafs, B. D. A., Püttmann, W., Sluijs, A., van Helmond, N. A. G. M., Vellekoop, J., Wagner, T., and Wrobel, N. E.:
1081 Cretaceous sea-surface temperature evolution: Constraints from TEX86 and
1082 planktonic foraminiferal oxygen isotopes, *Earth-Science Reviews*, 172, 224-247,
1083 <https://doi.org/10.1016/j.earscirev.2017.07.012>, 2017.
1084

1085 O'Regan, M., Moran, K., Sangiorgi, F., Brinkhuis, H., Backman, J., Jakobsson, M.,
1086 Stickley, C. E., Koc, N., Brumsack, H., Willard, D., Pockalny, R., and Skelton, A.:
1087 Mid-Cenozoic Tectonic and Paleoenvironmental setting of the Central Arctic
1088 Ocean, *Paleoceanography*, 23, PA1S20, doi:10.1029/2007PA001559, 2008.
1089

1090 Pagani, M., Pedentchouk, N., Huber, M., Sluijs, A., Schouten, S., Brinkhuis, H.,
1091 Sinninghe Damsté, J. S., Dickens, G. R., and Expedition 302 Scientists, T.: Arctic
1092 hydrology during global warming at the Palaeocene-Eocene thermal maximum,
1093 *Nature*, 442, 671-675, 2006.
1094

1095 Park, E., Hefter, J., Fischer, G., Iversen, M. H., Ramondenc, S., Nöthig, E. M., and
1096 Mollenhauer, G.: Seasonality of archaeal lipid flux and GDGT-based thermometry
1097 in sinking particles of high-latitude oceans: Fram Strait (79°N) and Antarctic Polar
1098 Front (50°S), *Biogeosciences*, 16, 2247-2268, 10.5194/bg-16-2247-2019, 2019.
1099

1100 Pierrehumbert, R. T.: The hydrologic cycle in deep-time climate problems, *Nature*, 419,
1101 191-198, 2002.
1102

1103 Pitcher, A., Hopmans, E. C., Mosier, A. C., Park, S.-J., Rhee, S.-K., Francis, C. A.,
1104 Schouten, S., and Sinninghe Damsté, J. S.: Core and Intact Polar Glycerol
1105 Dibiphytanyl Glycerol Tetraether Lipids of Ammonia-Oxidizing Archaea
1106 Enriched from Marine and Estuarine Sediments, *Applied and Environmental
1107 Microbiology*, 77, 3468-3477, 10.1128/aem.02758-10, 2011a.
1108

1109 Pitcher, A., Wuchter, C., Siedenberg, K., Schouten, S., and Sinninghe Damsté, J. S.:
1110 Crenarchaeol tracks winter blooms of ammonia-oxidizing Thaumarchaeota in the
1111 coastal North Sea, *Limnol Oceanogr*, 56, 2308-2318, 10.4319/lo.2011.56.6.2308,
1112 2011b.
1113

1114 Qin, W., Amin, S. A., Martens-Habbena, W., Walker, C. B., Urakawa, H., Devol, A.
1115 H., Ingalls, A. E., Moffett, J. W., Armbrust, E. V., and Stahl, D. A.: Marine
1116 ammonia-oxidizing archaeal isolates display obligate mixotrophy and wide
1117 ecotypic variation, *Proceedings of the National Academy of Sciences*, 111, 12504-
1118 12509, 10.1073/pnas.1324115111, 2014.
1119

1120 Qin, W., Carlson, L. T., Armbrust, E. V., Devol, A. H., Moffett, J. W., Stahl, D. A., and
1121 Ingalls, A. E.: Confounding effects of oxygen and temperature on the TEX₈₆
1122 signature of marine Thaumarchaeota, *Proceedings of the National Academy of
1123 Sciences*, 112, 10979-10984, 10.1073/pnas.1501568112, 2015.
1124

1125 Reichgelt, T., West, C. K., and Greenwood, D. R.: The relation between global palm
1126 distribution and climate, *Scientific Reports*, 8, 4721, 10.1038/s41598-018-23147-
1127 2, 2018.
1128

1129 Richey, J. N., and Tierney, J. E.: GDGT and alkenone flux in the northern Gulf of
1130 Mexico: Implications for the TEX86 and UK'37 paleothermometers,
1131 *Paleoceanography*, 31, 1547-1561, 10.1002/2016pa003032, 2016.
1132

1133 Sangiorgi, F., van Soelen, E. E., Spofforth, D. J. A., Pälike, H., Stickley, C. E., St. John,
1134 K., Koç, N., Schouten, S., Sinninghe Damsté, J. S., and Brinkhuis, H.: Cyclicity in
1135 the middle Eocene central Arctic Ocean sediment record: Orbital forcing and
1136 environmental response, *Paleoceanography*, 23, n/a-n/a, 10.1029/2007PA001487,
1137 2008.
1138

1128 Schouten, S., Hopmans, E. C., Schefuß, E., and Sinninghe Damsté, J. S.: Distributional
1129 variations in marine crenarchaeotal membrane lipids: a new tool for reconstructing
1130 ancient sea water temperatures?, *Earth and Planetary Science Letters*, 204, 265-
1131 274, 2002.

1132 Schouten, S., Hopmans, E. C., Forster, A., Breugel, Y. V., Kuypers, M. M. M., and
1133 Sinninghe Damsté, J. S.: Extremely high sea-surface temperatures at low latitudes
1134 during the middle Cretaceous as revealed by archaeal membrane lipids, *Geology*,
1135 31, 1069-1072, 2003.

1136 Schouten, S., Forster, A., Panoto, F. E., and Sinninghe Damste, J. S.: Towards
1137 calibration of the TEX86 palaeothermometer for tropical sea surface temperatures
1138 in ancient greenhouse worlds, *Org Geochem*, 38, 1537-1546, 2007a.

1139 Schouten, S., Baas, M., Hopmans, E. C., and Sinninghe Damsté, J. S.: An unusual
1140 isoprenoid tetraether lipid in marine and lacustrine sediments, *Org Geochem*, 39,
1141 1033-1038, 2008.

1142 Schouten, S., Hopmans, E. C., Meer, J. v. d., Mets, A., Bard, E., Bianchi, T. S.,
1143 Diefendorf, A., Escala, M., Freeman, K. H., Furukawa, Y., Ingalls, C. H. a. A.,
1144 Ménot-Combes, G., Nederbragt, A. J., Oba, M., Pearson, A., Pearson, E. J., Rosell-
1145 Melé, A., Schaeffer, P., Shah, S. R., Shanahan, T. M., Smith, R. W., Smittenberg,
1146 R., Talbot, H. M., Uchida, M., Mooy, B. A. S. V., Yamamoto, M., Zhang, Z., and
1147 Sinninghe Damsté, J. S.: An interlaboratory study of TEX86 and BIT analysis
1148 using high-performance liquid chromatography-mass spectrometry, *Geochemistry
1149 Geophysics Geosystems*, 10, Q03012, doi:03010.01029/02008GC002221, 2009.

1150 Schouten, S., Hopmans, E. C., and Sinninghe Damsté, J. S.: The organic geochemistry
1151 of glycerol dialkyl glycerol tetraether lipids: A review, *Org Geochem*, 54, 19-61,
1152 <http://dx.doi.org/10.1016/j.orggeochem.2012.09.006>, 2013.

1153 Schweitzer, H.-J.: Environment and climate in the early Tertiary of Spitsbergen,
1154 *Palaeogeography, Palaeoclimatology, Palaeoecology*, 30, 297-311, 1980.

1155 Seton, M., Müller, R. D., Zahirovic, S., Gaina, C., Torsvik, T., Shephard, G., Talsma,
1156 A., Gurnis, M., Turner, M., Maus, S., and Chandler, M.: Global continental and
1157 ocean basin reconstructions since 200Ma, *Earth-Science Reviews*, 113, 212-270,
1158 <https://doi.org/10.1016/j.earscirev.2012.03.002>, 2012.

1159 Shah, S. R., Mollenhauer, G., Ohkouchi, N., Eglinton, T. I., and Pearson, A.: Origins
1160 of archaeal tetraether lipids in sediments: Insights from radiocarbon analysis,
1161 *Geochim Cosmochim Ac*, 72, 4577-4594,
1162 <https://doi.org/10.1016/j.gca.2008.06.021>, 2008.

1163 Sinninghe Damsté, J. S., Wakeham, S. G., Kohnen, M. E. L., Hayes, J. M., and de
1164 Leeuw, J. W.: A 6,000-year sedimentary molecular record of chemocline
1165 excursions in the Black Sea, *Nature*, 362, 827 - 829, 1993.

1166 Sinninghe Damsté, J. S., Rijpstra, W. I. C., Hopmans, E. C., Weijers, J. W. H., Foesel,
1167 B. U., Overmann, J., and Dedysh, S. N.: 13,16-Dimethyl Octacosanedioic Acid
1168 (*iso*-Diabolic Acid), a Common Membrane-Spanning Lipid of Acidobacteria
1169 Subdivisions 1 and 3, *Applied and Environmental Microbiology*, 77, 4147-4154,
1170 10.1128/aem.00466-11, 2011.

1171 Sinninghe Damsté, J. S.: Spatial heterogeneity of sources of branched tetraethers in
1172 shelf systems: The geochemistry of tetraethers in the Berau River delta
1173 (Kalimantan, Indonesia), *Geochim Cosmochim Ac*, 186, 13-31,
1174 <https://doi.org/10.1016/j.gca.2016.04.033>, 2016.

1175 Sinninghe Damsté, J. S., Rijpstra, W. I. C., Foesel, B. U., Huber, K. J., Overmann, J.,
1176 Nakagawa, S., Kim, J. J., Dunfield, P. F., Dedysh, S. N., and Villanueva, L.: An
1177 overview of the occurrence of ether- and ester-linked *iso*-diabolic acid membrane

1178 lipids in microbial cultures of the Acidobacteria: Implications for brGDGT
1179 paleoproxies for temperature and pH, *Org Geochem*, 124, 63-76,
1180 <https://doi.org/10.1016/j.orggeochem.2018.07.006>, 2018a.

1181 Sinninghe Damsté, J. S., Rijpstra, W. I. C., Hopmans, E. C., den Uijl, M. J., Weijers, J.
1182 W. H., and Schouten, S.: The enigmatic structure of the crenarchaeol isomer, *Org*
1183 *Geochem*, 124, 22-28, <https://doi.org/10.1016/j.orggeochem.2018.06.005>, 2018b

1184 Sluijs, A., Schouten, S., Pagani, M., Woltering, M., Brinkhuis, H., Sinninghe Damsté,
1185 J. S., Dickens, G. R., Huber, M., Reichart, G.-J., Stein, R., Matthiessen, J., Lourens,
1186 L. J., Pedentchouk, N., Backman, J., Moran, K., and The Expedition 302 Scientists:
1187 Subtropical Arctic Ocean temperatures during the Palaeocene/Eocene thermal
1188 maximum, *Nature*, 441, 610-613, 2006.

1189 Sluijs, A., Brinkhuis, H., Crouch, E. M., John, C. M., Handley, L., Munsterman, D.,
1190 Bohaty, S., M., Zachos, J. C., Reichart, G.-J., Schouten, S., Pancost, R. D.,
1191 Sinninghe Damsté, J. S., Welters, N. L. D., Lotter, A. F., and Dickens, G. R.:
1192 Eustatic variations during the Paleocene-Eocene greenhouse world,
1193 *Paleoceanography*, 23, PA4216, doi:10.1029/2008PA001615, 2008a.

1194 Sluijs, A., Röhl, U., Schouten, S., Brumsack, H.-J., Sangiorgi, F., Sinnenhe Damsté, J.
1195 S., and Brinkhuis, H.: Arctic late Paleocene-early Eocene paleoenvironments with
1196 special emphasis on the Paleocene-Eocene thermal maximum (Lomonosov Ridge,
1197 Integrated Ocean Drilling Program Expedition 302), *Paleoceanography*, 23,
1198 PA1S11, doi:10.1029/2007PA001495, 2008b.

1199 Sluijs, A., Schouten, S., Donders, T. H., Schoon, P. L., Röhl, U., Reichart, G. J.,
1200 Sangiorgi, F., Kim, J.-H., Sinnenhe Damsté, J. S., and Brinkhuis, H.: Warm and
1201 Wet Conditions in the Arctic Region during Eocene Thermal Maximum 2, *Nature*
1202 *Geoscience*, 2, 777-780, 2009.

1203 Sluijs, A., and Dickens, G. R.: Assessing offsets between the $\delta^{13}\text{C}$ of sedimentary
1204 components and the global exogenic carbon pool across Early Paleogene carbon
1205 cycle perturbations, *Global Biogeochemical Cycles*, 26, GB4005,
1206 doi:10.1029/2011GB004224, 2012.

1207 Sollich, M., Yoshinaga, M. Y., Häusler, S., Price, R. E., Hinrichs, K.-U., and Bühring,
1208 S. I.: Heat Stress Dictates Microbial Lipid Composition along a Thermal Gradient
1209 in Marine Sediments, *Frontiers in Microbiology*, 8, 10.3389/fmicb.2017.01550,
1210 2017.

1211 Spielhagen, R. F., and Tripati, A.: Evidence from Svalbard for near-freezing
1212 temperatures and climate oscillations in the Arctic during the Paleocene and
1213 Eocene, *Palaeogeography, Palaeoclimatology, Palaeoecology*, 278, 48-56,
1214 <https://doi.org/10.1016/j.palaeo.2009.04.012>, 2009.

1215 Stein, R., Boucsein, B., and Meyer, H.: Anoxia and high primary production in the
1216 Paleogene central Arctic Ocean: First detailed records from Lomonosov Ridge,
1217 *Geophysical Research Letters*, 33, L18606, doi:10.1029/2006GL026776, 2006.

1218 Stein, R.: Upper Cretaceous/lower Tertiary black shales near the North Pole: Organic-
1219 carbon origin and source-rock potential, *Marine and Petroleum Geology*, 24, 67-
1220 73, 2007.

1221 Suan, G., Popescu, S.-M., Yoon, D., Baudin, F., Suc, J.-P., Schnyder, J., Labrousse, L.,
1222 Fauquette, S., Piepjohn, K., and Sobolev, N. N.: Subtropical climate conditions and
1223 mangrove growth in Arctic Siberia during the early Eocene, *Geology*, 45, 539-542,
1224 10.1130/g38547.1, 2017.

1225 Taylor, K. W. R., Huber, M., Hollis, C. J., Hernandez-Sanchez, M. T., and Pancost, R.
1226 D.: Re-evaluating modern and Palaeogene GDGT distributions: Implications for

1227 SST reconstructions, *Global and Planetary Change*, 108, 158-174,
1228 <http://dx.doi.org/10.1016/j.gloplacha.2013.06.011>, 2013.

1229 Teichert, B. M. A., and Luppold, F. W.: Glendonites from an Early Jurassic methane
1230 seep — Climate or methane indicators?, *Palaeogeography, Palaeoclimatology,*
1231 *Palaeoecology*, 390, 81-93, <https://doi.org/10.1016/j.palaeo.2013.03.001>, 2013.

1232 Tierney, J. E., and Tingley, M. P.: A Bayesian, spatially-varying calibration model for
1233 the TEX86 proxy, *Geochim Cosmochim Ac*, 127, 83-106,
1234 <http://dx.doi.org/10.1016/j.gca.2013.11.026>, 2014.

1235 Tierney, J. E., Sinninghe Damst , J. S., Pancost, R. D., Sluijs, A., and Zachos, J. C.:
1236 Eocene temperature gradients, *Nature Geosci*, 10, 538-539, 10.1038/ngeo2997,
1237 2017.

1238 Torsvik, T. H., Van der Voo, R., Preeden, U., Mac Niocaill, C., Steinberger, B.,
1239 Doubrovine, P. V., van Hinsbergen, D. J. J., Domeier, M., Gaina, C., Tohver, E.,
1240 Meert, J. G., McCausland, P. J. A., and Cocks, L. R. M.: Phanerozoic polar wander,
1241 palaeogeography and dynamics, *Earth-Science Reviews*, 114, 325-368,
1242 <https://doi.org/10.1016/j.earscirev.2012.06.007>, 2012.

1243 Trommer, G., Siccha, M., van der Meer, M. T. J., Schouten, S., Sinninghe Damst , J.
1244 S., Schulz, H., Hemleben, C., and Kucera, M.: Distribution of Crenarchaeota
1245 tetraether membrane lipids in surface sediments from the Red Sea, *Org Geochem*,
1246 40, 724-731, <https://doi.org/10.1016/j.orggeochem.2009.03.001>, 2009.

1247 Uhl, D., Traiser, C., Griesser, U., and Denk, T.: Fossil leaves as palaeoclimate proxies
1248 in the Palaeogene of Spitsbergen (Svalbard), *Acta Palaeobotanica*, 47, 89-107,
1249 2007.

1250 Van der Burgh, J.: Some palms in the Miocene of the lower Rhenish Plain, *Review of
1251 Palaeobotany and Palynology*, 40, 359-374, 1984.

1252 Van Hinsbergen, D. J. J., de Groot, L. V., van Schaik, S. J., Spakman, W., Bijl, P. K.,
1253 Sluijs, A., Langereis, C. G., and Brinkhuis, H.: A Paleolatitude Calculator for
1254 Paleoclimate Studies, *PLOS ONE*, 10, e0126946, 10.1371/journal.pone.0126946,
1255 2015.

1256 Wakeham, S. G., Amann, R., Freeman, K. H., Hopmans, E. C., J rgensen, B. B.,
1257 Putnam, I. F., Schouten, S., Sinninghe Damst , J. S., Talbot, H. M., and Woebken,
1258 D.: Microbial ecology of the stratified water column of the Black Sea as revealed
1259 by a comprehensive biomarker stud, *Org Geochem*, 38, 2070-2097, 2007.

1260 Weijers, J. W. H., Schouten, S., Spaargaren, O. C., and Sinninghe Damst , J. S.:
1261 Occurrence and distribution of tetraether membrane lipids in soils: Implications for
1262 the use of the TEX86 proxy and the BIT index, *Org Geochem*, 37, 1680-1693,
1263 2006.

1264 Weijers, J. W. H., Schouten, S., Sluijs, A., Brinkhuis, H., and Sinninghe Damst , J. S.:
1265 Warm arctic continents during the Palaeocene-Eocene thermal maximum, *Earth
1266 and Planetary Science Letters*, 261, 230-238, 2007a.

1267 Weijers, J. W. H., Schouten, S., van den Donker, J. C., Hopmans, E. C., and Sinninghe
1268 Damst , J. S.: Environmental controls on bacterial tetraether membrane lipid
1269 distribution in soils, *Geochim Cosmochim Ac*, 71, 703-713, 2007b.

1270 Weijers, J. W. H., Lim, K. L. H., Aquilina, A., Sinninghe Damst , J. S., and Pancost,
1271 R. D.: Biogeochemical controls on glycerol dialkyl glycerol tetraether lipid
1272 distributions in sediments characterized by diffusive methane flux, *Geochemistry,
1273 Geophysics, Geosystems*, 12, doi:10.1029/2011GC003724, 2011.

1274 Willard, D. A., Donders, T. H., Reichgelt, T., Greenwood, D. R., Sangiorgi, F., Peterse,
1275 F., Nierop, K. G. J., Frieling, J., Schouten, S., and Sluijs, A.: Arctic vegetation,
1276 temperature, and hydrology during Early Eocene transient global warming events,

1277 Global and Planetary Change, 178, 139-152,
1278 <https://doi.org/10.1016/j.gloplacha.2019.04.012>, 2019.

1279 Wuchter, C., Schouten, S., Coolen, M. J. L., and Sinninghe Damsté, J. S.: Temperature-
1280 dependent variation in the distribution of tetraether membrane lipids of marine
1281 Crenarchaeota: Implications for TEX86 paleothermometry, *Paleoceanography*, 19,
1282 PA402, 2004.

1283 Wuchter, C., Schouten, S., Wakeham, S. G., and Sinninghe Damste, J. S.: Temporal
1284 and spatial variation in tetraether membrane lipids of marine Crenarchaeota in
1285 particulate organic matter: Implications for TEX86 paleothermometry,
1286 *Paleoceanography*, 20, doi:10.1029/2004PA001110, 2005.

1287 Wuchter, C., Abbas, B., Coolen, M. J. L., Herfort, L., van Bleijswijk, J., Timmers, P.,
1288 Strous, M., Teira, E., Herndl, G. J., Middelburg, J. J., Schouten, S., and Damste, J.
1289 S. S.: Archaeal nitrification in the ocean, *Proceedings of the National Academy of
1290 Sciences of the United States of America*, 103, 12317-12322,
1291 10.1073/pnas.0600756103, 2006a.

1292 Wuchter, C., Schouten, S., Wakeham, S. G., and Sinninghe Damsté, J. S.: Archaeal
1293 tetraether membrane lipid fluxes in the northeastern Pacific and the Arabian Sea:
1294 Implications for TEX86 paleothermometry, *Paleoceanography*, 21, PA4208,
1295 2006b.

1296 Xie, S., Liu, X.-L., Schubotz, F., Wakeham, S. G., and Hinrichs, K.-U.: Distribution of
1297 glycerol ether lipids in the oxygen minimum zone of the Eastern Tropical North
1298 Pacific Ocean, *Org Geochem*, 71, 60-71,
1299 <https://doi.org/10.1016/j.orggeochem.2014.04.006>, 2014.

1300 Yamamoto, M., Shimamoto, A., Fukuhara, T., Tanaka, Y., and Ishizaka, J.: Glycerol
1301 dialkyl glycerol tetraethers and TEX86 index in sinking particles in the western
1302 North Pacific, *Org Geochem*, 53, 52-62,
1303 <https://doi.org/10.1016/j.orggeochem.2012.04.010>, 2012.

1304 Zeng, Z., Liu, X.-L., Farley, K. R., Wei, J. H., Metcalf, W. W., Summons, R. E., and
1305 Welander, P. V.: GDGT cyclization proteins identify the dominant archaeal
1306 sources of tetraether lipids in the ocean, *Proceedings of the National Academy of
1307 Sciences*, 116, 22505-22511, 10.1073/pnas.1909306116, 2019.

1308 Zhang, Y. G., Zhang, C. L., Liu, X.-L., Li, L., Hinrichs, K.-U., and Noakes, J. E.:
1309 Methane Index: A tetraether archaeal lipid biomarker indicator for detecting the
1310 instability of marine gas hydrates, *Earth and Planetary Science Letters*, 307, 525-
1311 534, <https://doi.org/10.1016/j.epsl.2011.05.031>, 2011.

1312 Zhang, Y. G., Pagani, M., and Wang, Z.: Ring Index: A new strategy to evaluate the
1313 integrity of TEX86 paleothermometry, *Paleoceanography*, 31, 220-232,
1314 doi:10.1002/2015PA002848, 2016.

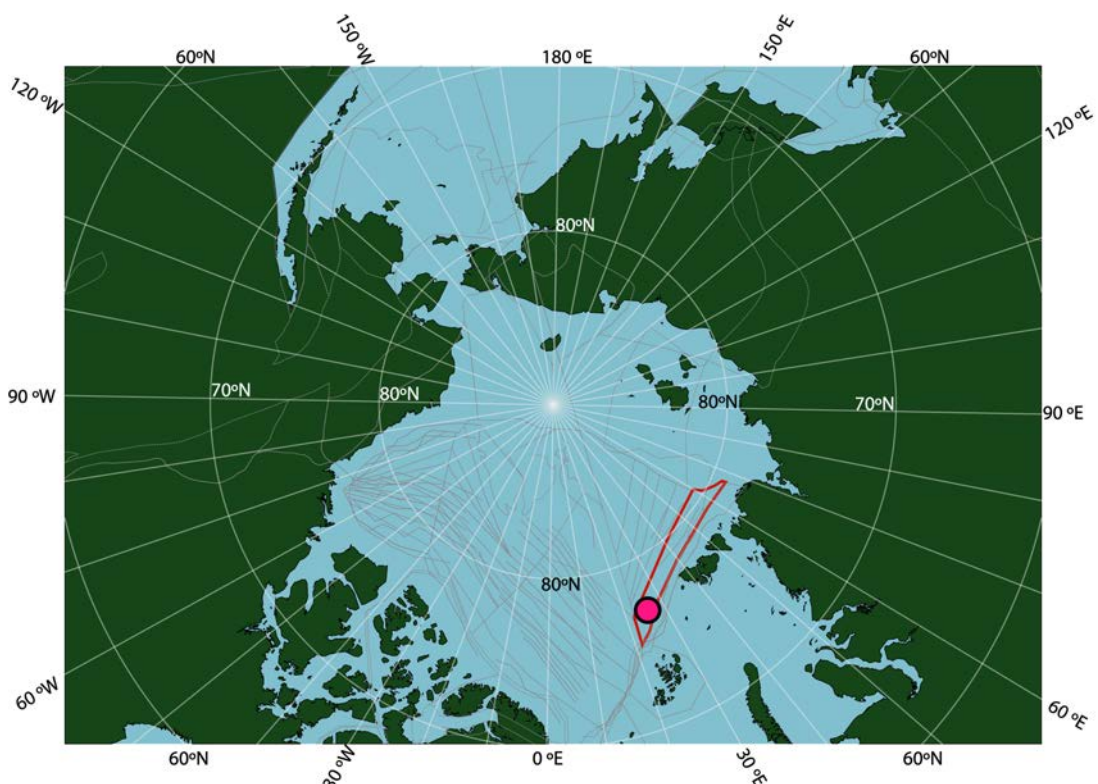
1315 Zhang, Y. G., and Liu, X.: Export Depth of the TEX86 Signal, *Paleoceanography and
1316 Paleoclimatology*, 33, 666-671, 10.1029/2018pa003337, 2018.

1317 Zhu, J., Poulsen, C. J., and Tierney, J. E.: Simulation of Eocene extreme warmth and
1318 high climate sensitivity through cloud feedbacks, *Science Advances*, 5, eaax1874,
1319 10.1126/sciadv.aax1874, 2019.

1320

1321 **Figure 1.** Location of ACEX Hole 4A within a paleogeographic reconstruction of the
1322 Arctic region at the time of the PETM. Reconstruction made using gplates (Müller et
1323 al., 2018), with the tectonic reconstruction of Seton et al. (2012, red shape is
1324 Lomonosov Ridge in this reconstruction and grey lines are structural features including
1325 spreading ridges), the paleomagnetic reference frame of Torsvik et al., (2012), and
1326 modern coastlines.

1327

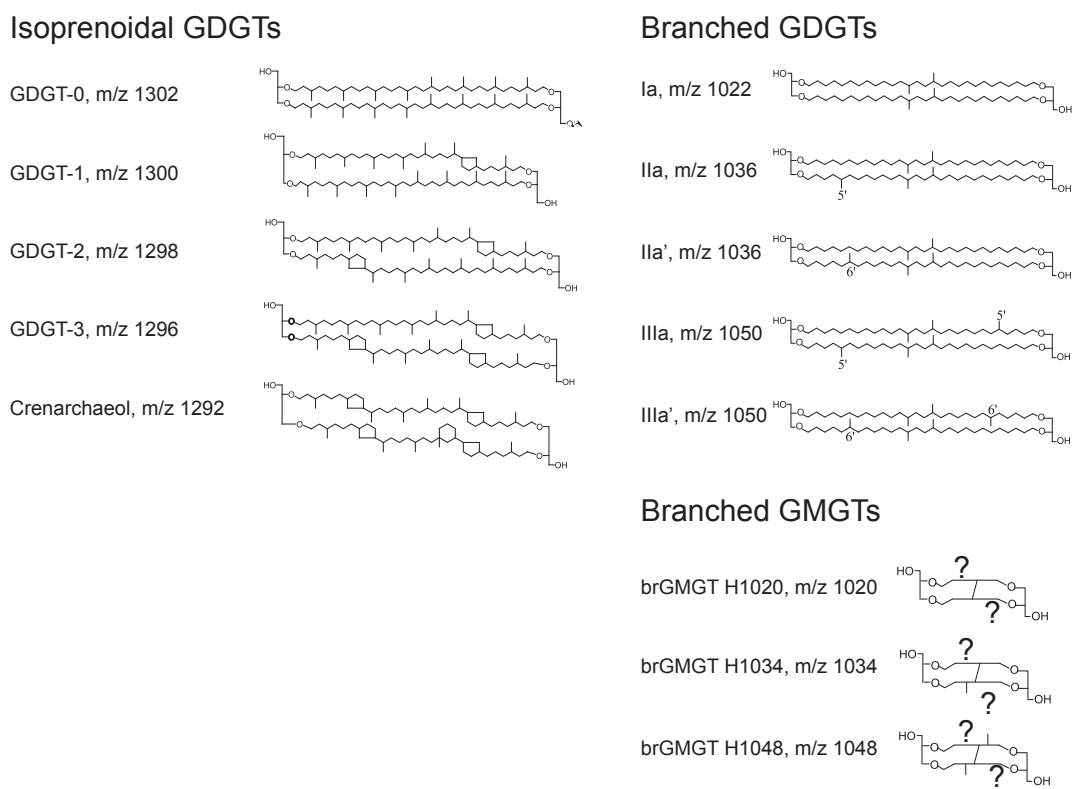


1328

1329

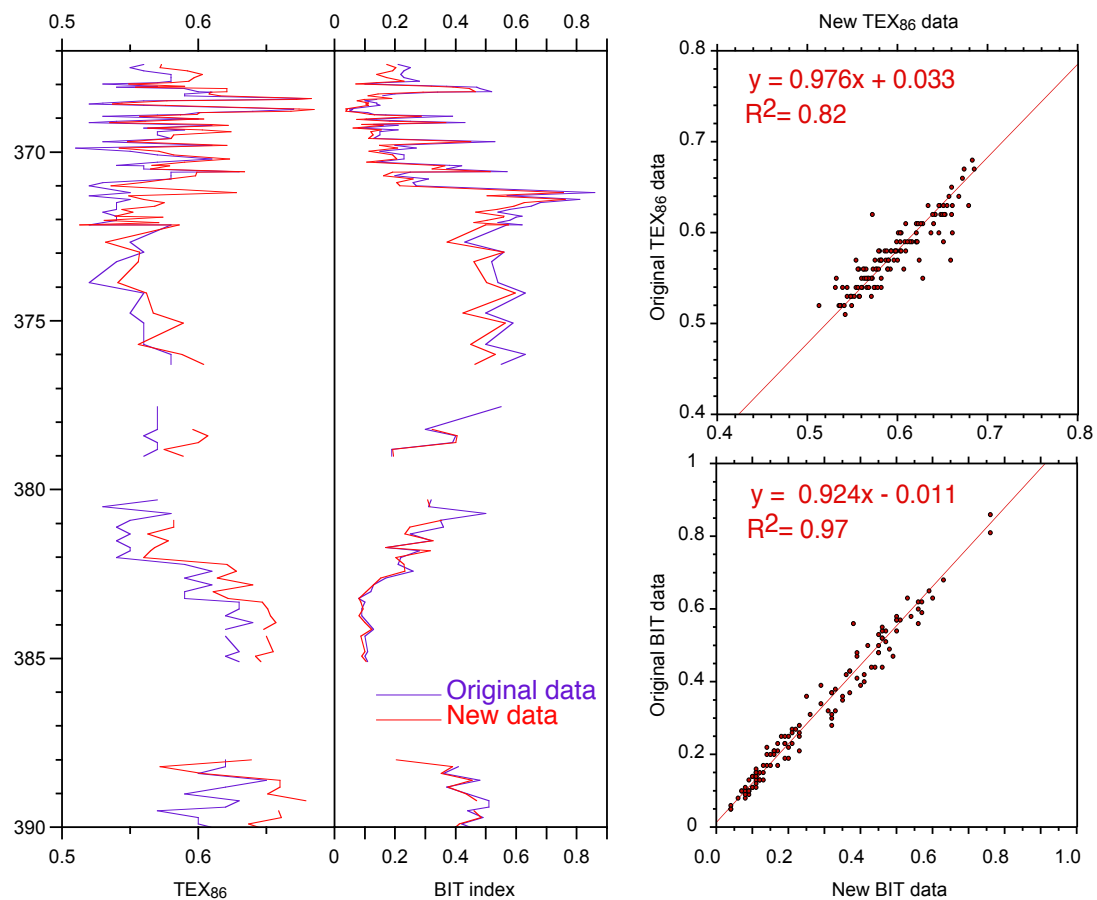
1330 **Figure 2.** Molecular structures of the relevant isoGDGTs, brGDGTs and brGMGTs
 1331 and their terminology as described in this study. Crenarchaeol isomer (not shown)
 1332 differs from Crenarchaeol in the stereochemistry of the cyclopentane moiety adjacent
 1333 to the cyclohexyl moiety (Sinninghe Damsté et al., 2018b). For the terminology of the
 1334 brGMGTs, for which the exact chemical structure is still unclear, we follow Baxter et
 1335 al. (2019), since we identify the same isomers (see Figure S2 for a chromatogram).

1336



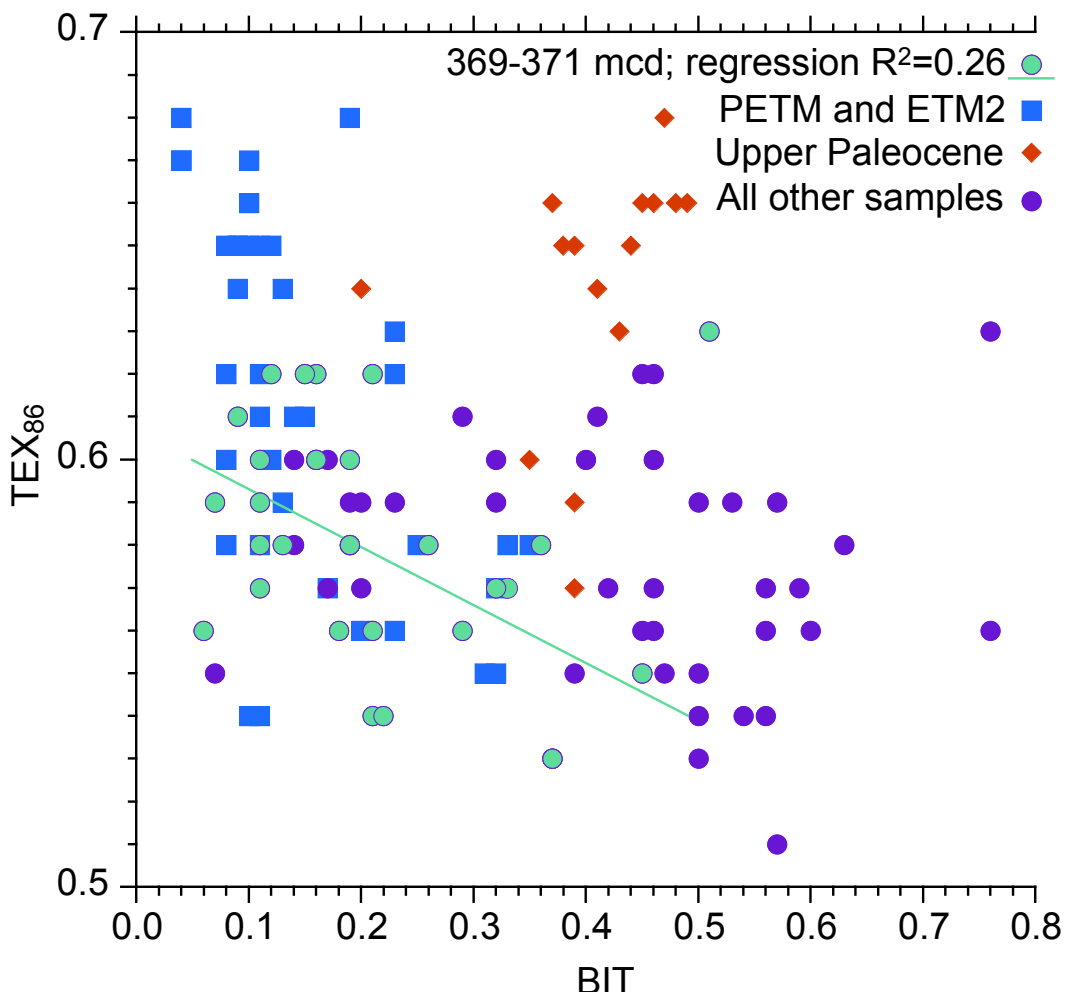
1337

1338 **Figure 3.** Comparison of the original GDGT dataset of the upper Paleocene and lower
1339 Eocene of ACEX Hole 4A (Sluijs et al., 2006; Sluijs et al., 2009) and the new data
1340 generated according to the latest chromatography protocols.



1341

1342 **Figure 4.** Comparison between BIT index values and TEX_{86} for various intervals
1343 spanning the upper Paleocene and lower Eocene of ACEX Hole 4A.



1344

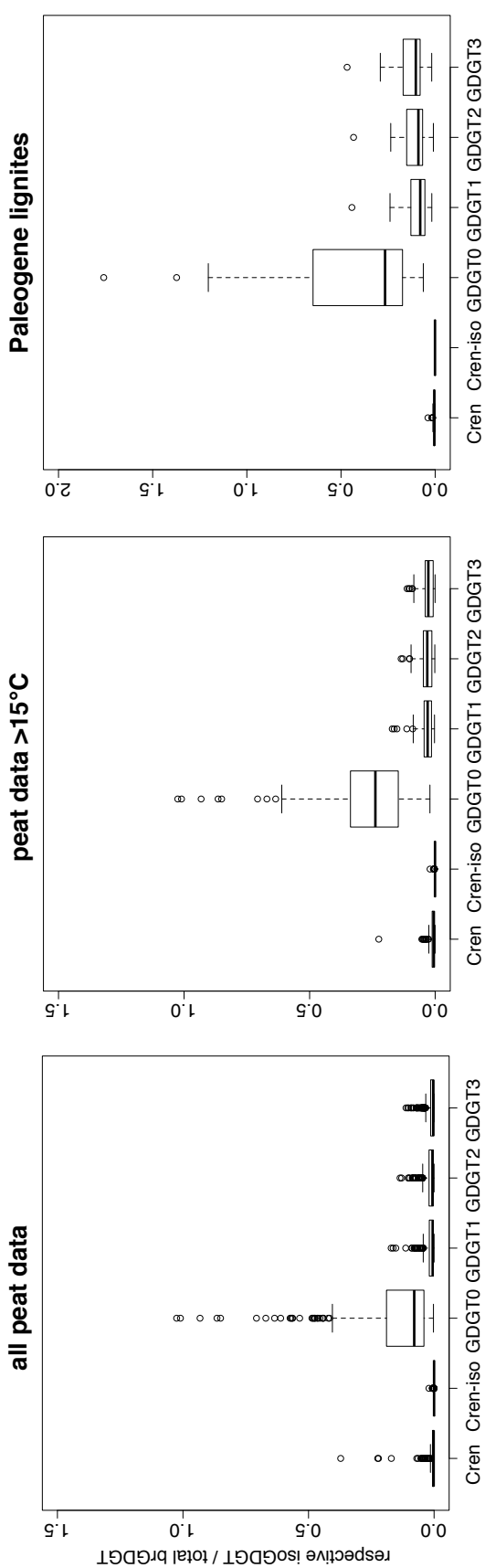


Figure 5. The abundance of various isoGDGTs relative to the total brGDGT abundance in modern peats (left 2 panels) and Paleogene lignites (right panel; Equation 9), used to assess potential isoGDGT contributions to the ACEX samples. The box is standard 25%-50%-75% quantiles, whiskers represent box limits plus/minus $1.5 \times$ the interquartile range (IQR). Any data outside that range is given as circles. Number of measurements per dataset: Modern peats = 473 (most isoGDGTs have been identified in ± 430 of those; Modern peats above 15°C = 141 (all except one of there have isoGDGT data; Lignites = 58 (allof which have isoGDGT data but only 29 have available (quantifiable) crenarchaeol isomer data).

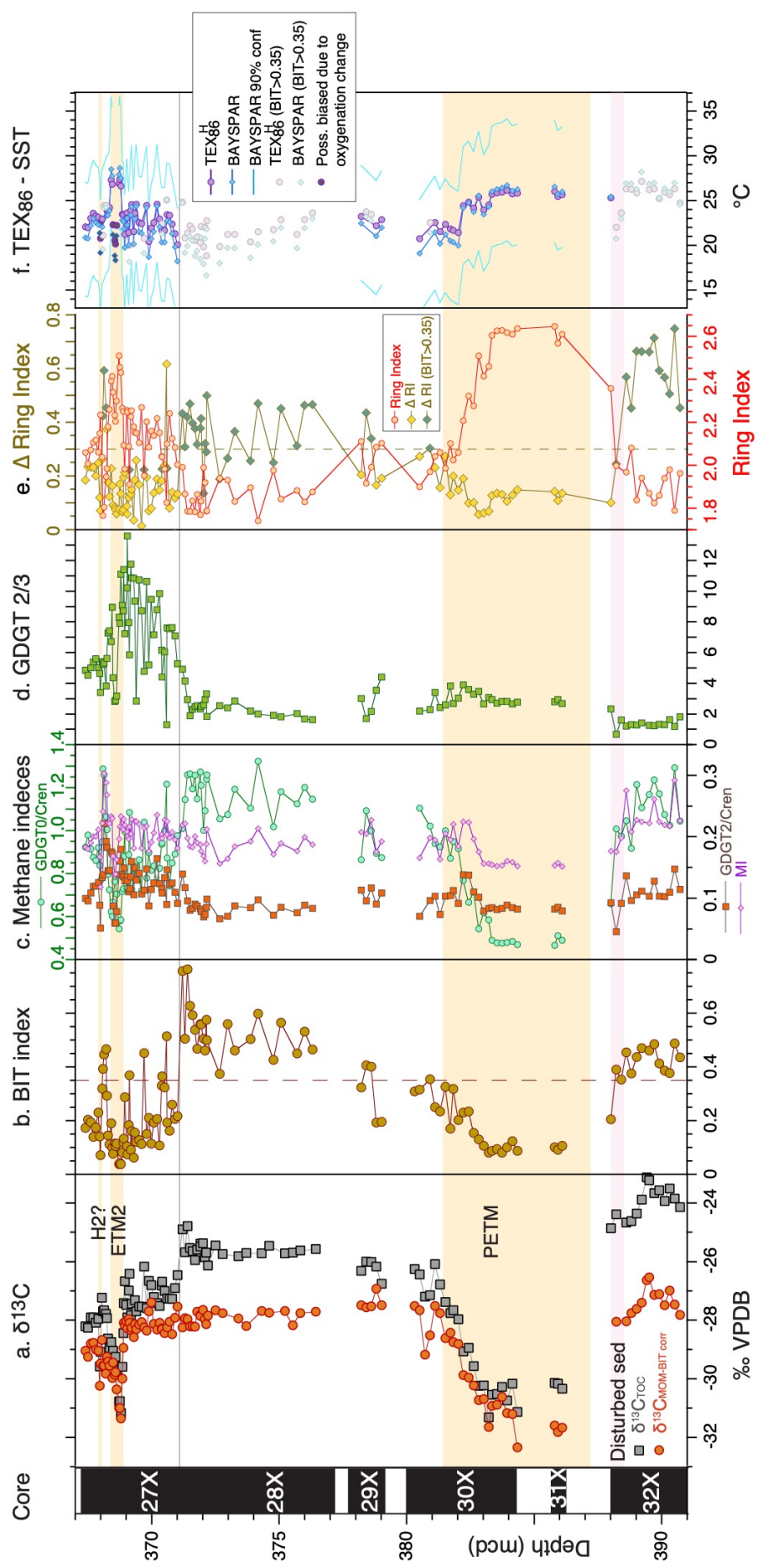


Figure 6. Branched and Isoprenoid GDGT records across the upper Paleocene and lower Eocene of ACEX Hole 4A. a. carbon isotope stratigraphy (total organic carbon record from Sluijs et al., 2006 and 2009; marine organic matter record from Sluijs and Dickens (2012)), b. BIT index (equation 2), c. indices indicative of anaerobic archaeal methanotrophy (MI index (equation 3) and GDGT-2/Crenarchaeol), and methanogenesis (GDGT-0/Crenarchaeol), d. GDGT2-GDGT3 ratio, e. Ring index (equation 5) and Δ Ring Index, f. TEX86 (equation 1) calibrated to sea surface temperature using a non-linear calibration TEX_86^H calibration (Kim et al., 2010) and the BAYSPAR method, which is based on a linear calibration (Tierney and Tingley, 2014).

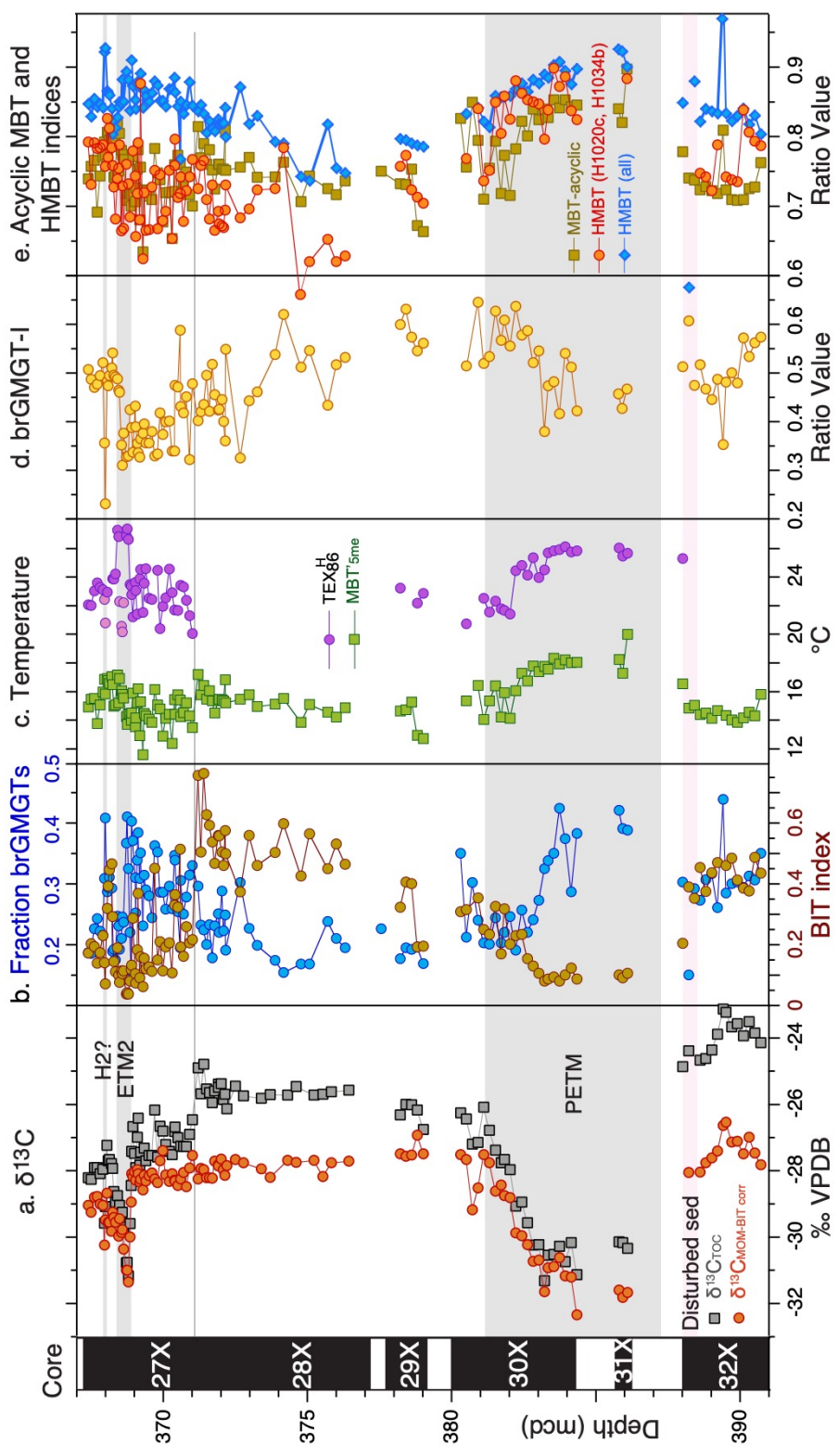


Figure 7. Branched GMGT records across the upper Paleocene and lower Eocene of ACEX Hole 4A. a. carbon isotope stratigraphy (total organic carbon record from Sluijs et al., 2006 and 2009; marine organic matter record from Sluijs and Dickens (2012)), b. fraction of br-GMGTs of the total branched GDGTs and GMGTs and BIT index (equation 2), c. MBT- ^{57}Fe record (Willard et al., 2019) and TEX_{86}^H , d. MBT_{acyclic} (equation 6) and H-MBT based on all isomers detected with m/z 1020 and m/z 1034 (H-MBT all; equation 7) and based on H1020a and H1034b (H-MBT H1020a, H1034c), e. brGMGT-1 record (equation 8).